Anthraquinone Laxative-Altered Gut Microbiota Induces Colonic Mucosal Barrier Dysfunction for Colorectal Cancer Progression

Zhonghong Wei
Nanjing University of Chinese Medicine
Jiawei Wu
Nanjing University of Chinese Medicine
Yu Yang
Nanjing University of Chinese Medicine
Peiliang Shen
Nanjing University of Chinese Medicine
Peng Cheng
Nanjing University of Chinese Medicine
Li Tao
Yangzhou University
Yunlong Shan
China Pharmaceutical University
Zhiguang Sun
Nanjing University of Chinese Medicine
Yin Lu (luyingreen@njucm.edu.cn)
Nanjing University of Chinese Medicine https://orcid.org/0000-0003-2063-8485

Research

Keywords: Anthraquinone laxative, sennoside A, gut microbiota, Akkermansia muciniphila, colonic mucosal barrier, colitis-associated colon cancer

Posted Date: September 10th, 2020

DOI: https://doi.org/10.21203/rs.3.rs-72368/v1

Abstract

Background: The safety of anthraquinone laxatives has been controversial. Previously, a few scattered studies have revealed that anthraquinones can cause the damage to the structure of colonic epithelial tissue, and long-term intake of anthraquinone laxatives increase the colorectal cancer risks. In this study, we focused on sennoside A, a primary purgative component in anthraquinone laxatives, and investigated the effects of sennoside A on intestinal inflammation, host metabolism, and whether it can exacerbate the colitis-associated colon cancer in the AOM/DSS mouse model.

Results: Initially, sennoside A disrupted the mucus layer and mechanical barrier of the colon. The dynamic effects of sennoside A on the community structure of gut microbiota were futher anlyazed. We found sennoside A significantly promoted the dominant growth of *Akkermansia muciniphila* after continuous treatment for 56 days, which was independent of the prototype of sennoside A and its metabolites, including the main host metabolite rhein and bacteria metabolites. Interestingly, sennoside A suppressed the growth of butyrate-producing bacteria, thereby decreasing the butyrate levels. Besides, sennoside A directly inhibited the growth of *Clostridium tyrobutyrate* and *Clostridium butyricum,* which was not caused by the prototype of sennoside A , but the direct bacteriostatic effect produced from its metaboliterhein. Lastly, supplement with butyrate prevented sennoside A-induced gut dysbiosis and mucus barrier impairment.

Conclusions: our work reveals that sennoside A can impair the integrity of the intestinal mucosal barrier, which is closely related to the disruption of the structural balance between mucus-degrading bacteria and exogenous fibro-degrading bacteria, inducing long term low-grade inflammation, metabolic disorders associated with tumorigenesis, and consequently promoting the progression of colonic carcinogenesis in the AOM/DSS mouse model.

Introduction

Anthraquinone laxatives (*e.g.*, Senna) are commonly employed to relief chronic constipation and obesity in clinical practice and exist in a variety of herbal/health supplements[1, 2]. However, the safety of anthraquinone laxatives has been controversial. As early as 1984, Dufour P *et al.* pointed out that long-term (16 weeks) administration of sennoside A, a primary component of anthraquinone laxatives, could cause the damage to the intestinal mucosa, destroy the structure of the intestinal wall, and increase the risk of carcinogenesis in experimental mice[3]. Mori *et al.* also found that the 1,8-dihydroxyanthraquinone contained in rhubarb induced adenomatous hyperproliferation in the colonic and cecal epithelial layers[4]. A prospective study involving 1095 patients unearthed that long-term use of anthraquinone laxatives had a 3.04-fold risk of colorectal cancer, which was significantly higher than that of people who did not take this class of drugs[5], which also clearly indicated that anthraquinones-containing herb Senna has a considerable colon carcinogenic effect[6]. In addition, in 2001, the *National Institutes of Health* (U.S.) warned of the potential carcinogenic risk of long-term use of anthraquinone compound[7]. However, there is a lack of clear evidence whether anthraquinone laxatives contribute to the development of tumors.

Of note, intestinal microorganisms play an important role in colonic inflammation and the development of colon cancer, and intestinal mucosal barrier injury is a key initiator for intestinal microorganisms to promote the development of colon cancer[8, 9]. Once the integrity of the intestinal mucosal barrier is damaged, the bacteria and their metabolites in the intestinal lumen translocate to the intestinal lamina propria through the space between the epithelial cells and triggerthe adaptive immune response. During the process, the epithelial cells are stimulated to release cytokines such as IL-1, IL-6 and IL-23, *etc*. IL-23 further activates Th17 cells. Th17 cells release IL-17 and activate the STAT3 and NF-κB signaling pathways,which promote epithelial cell proliferation and invasion, and induce gene mutations, resulting in further destruction of mucosal integrity and aggravated inflammatory response[10–13]. Chronic inflammation of the colon is a critical step in promoting the advancement of colon cancer. Colon cancer development is the result of a combination of intestinal mucosal barrier damage and an imbalance in intestinal microbial homeostasis[12, 13]. Goblet cells formed by the differentiation of colonic epithelial cells continuously secrete and replenish to maintain the coverage of intestinal epithelial cells by the mucus layer to form the first line of defense and lubricate the intestine[8]. Mucus outer layer is the habitat of commensal microorganisms and the nutrient source of some microorganisms, and its microbial species and physiological functions can affect the microbial composition in the intestinal lumen[14].

Sennoside A is one of the representative components of anthraquinone laxatives, and gut microbes might play a significant role in the purgative mechanism of sennoside A, as sennoside A neend to be hydrolyzed in the presence of β-glucosidase, which can be secreted by gut microbes [2, 15]. We hypothesized that that sennoside A could interact with the intraluminal microbiota and potentially elevate the pro-inflammatory carcinogenic risk *in vivo*. In this study, we focused on the role of gut microbes in the integrity of the intestinal mucosal barrier to elucidate whether sennoside A could disrupt the integrity of the colonic epithelial barrier and promote the development of colitis and colon cancer.

Result

Result 1 SennosideA induces intestinal epithelial barrier damage to promote bacterial translocation

To determine whether sennoside A directly could induce colon cancer development, we first evaluated whether long-term administration of sennoside A had pathological effects on colon tissue *in vivo.* As shown in **Figure S1A**, the colon adenomas was not observed after continuous administration of various doses of sennoside A (25, 50, 100 mg/kg) for 84 days. Moreover, sennoside A hardly induced a large number of lymphocyte infiltration in colonic mucosal layer and heterotype (atypical) hyperplasia (**Figure S1B)**. The cross section of normal colonic mucosal crypts was daisy-like morphology [16], and distributed with goblet cells filled with large amounts of mucus (**Figure 1A**, as marked by asterisk). Sennoside A (~ 25 mg/kg) inhibited the filling of mucus in goblet cells and the infiltration of lymphocytes in the crypt. At a dose of ~50 mg/kg, the colonic mucosa revealed relaxed crypt arrangement, disappeared mucus, and increased lymphocyte crypt invasion. Sennoside A (100 mg/kg) significantly reduced the sum of crypt and increased the distance between the crypt base and mucosal muscles. Extensive infiltration of inflammatory cells (mainly granulocyte neutrophils) was observed in colonic crypt and submucosa in

mice treated with 100 mg/kg of sennoside A **(Figure 1A&B)**.Thus, sennoside A can lead to changes in the structure and morphology of colonic crypts without active inflammation and formation of visible adenoma in the colon.

The effect of sennoside A on the mechanical barrier of the colon was further evaluated. As shown in **Figure 1C&D**, sennoside A dose-dependently inhibited the expression of claudin-1, ZO-1, and E-cadherin in colonic epithelial tissues. To determine whether sennoside A impaired tight junction proteins in colonic epithelial cells, NCM-460 colonocytes were incubated with sennoside *ex vivo*. Sennoside A alone or in combination with discovered that with β-glucosidase had no direct effect on tight junctions between NCM-460 cells (**Figure S2**). The mucus layer is a dynamic barrier that is constantly replenished by the secretory activity of the goblet cells. Our analysis was restricted to the inner mucus layer, which is well preserved and thus more reliable while the outer layer is prone to be disordered from the diet composition and fixation procedure [17]. The thickness of inner mucus layer and the number of goblet cells were further evaluated (**Figure 1E**), mucus thickness could be significantly reduced by sennoside A, and the number of goblet cells/crypt was decreased.

Intestinal mucosal permeability changes accurately reflect the degree of damage to the intestinal mucosal barrier and are an important indicator for monitoring the integrity of colonic barrier function[18]. Subsequently, we applied FITC-labeled dextran (FD4) to measure the total intestinal permeability using *in vivo* imaging technology We found sennoside A resulted in the disruption of intestinal barrier function integrity. Compared with the control mice, sennoside A (100 mg/kg) diminished fluorescence intensity in the intestinal lumen and the fluorescence showed a diffusion-like distribution in the abdominal cavity **(shown in Figure 1F).** Further fluorescence imaging of the colonic epithelium revealed that sennoside A promoted FD4 leakage into colonic epithelial tissue (**Figure 1F**), accompanied by the increased content of FD4 in serum **(Figure 1G)**. The loss of tight junctions between some colonic epithelial cells further promoted bacterial translocation to the colonic epithelial layer and even invaded into the colonic recess [19]. As shown in **Figure 1H&I**, Sennoside A (100 mg/kg) promotes bacterial translocation from the intestinal lumen to the colonic epithelial layer. Taken together, our data indicate that sennoside A destroys the functional barrier of colonic mucosa, increases the permeability of colonic barrier and promotes the translocation of microorganisms in intestinal lumen.

Result 2 Sennoside A promotes the dominant growth of *Akkermansia muciniphila*

It has been pointed out that the gut microbiota involved in the integrity of the intestinal mucosal barrier is the initial link to the occurrence and development of colitis-associated colon cancer [13]. We performed 16s rDNA detection analysis of bacteria from mouse cecal contents. As shown in **Figure S3A&B**, sennoside A (100mg/kg) treatment for 84 days changed the microbial community structure and decreased microbial alpha-diversity in mice. Further analysis was performed to obtain the bacteria characteristics of the pathological phenotype generated by sennoside A. As shown in the **Figure 2A**, sennoside A significantly promoted the relative abundance of *Verrucomicrobia* and reduced the relative abundance of *Firmicutes,* while the *Akkermansia* was the only genus of *Verrucomicrobia* among colonic

microorganisms. The results of genus-level analysis indicated that relative abundance of *Akkermansia* genus was significantly promoted by Sennoside A (**Figure 2B and FigureS3C**).

In addition, linear discriminant analysis effect size (LEfSe) was used to identify that the representative taxons of Sennoside A group was *Akkermansia muciniphila* species under the *Verrucomicrobia* phylum, and the evolutionary clade diagram displayed consistent results (**Figure 2C**). Based on quantitative PCR, we observed that the absolute *A. muciniphila* count significantly increased following sennoside A treatment (**Figure 2D**). To further explore the effects of sennoside A on the dynamic growth of *A. muciniphila*, 16s rDNA sequencing was performed at different time points. The results showed that successive administration of sennoside A (100 mg/kg) for 56 days caused a dominant growth of *A. muciniphila* (**Figure 2E)**. However, the dominant growth of *A. muciniphila* did not occur immediately after sennoside A treatment. Presumably, sennoside A might not directly affect the growth of *A. muciniphila*.

To investigate whether sennoside A had a direct impact on the growth of *A.muciniphila*, bacterial growth was evaluated at OD600[20]**(Figure 2F)**. Sennoside A is metabolized by a variety of bacteria-drove hydrolytic enzymes in the intestinal lumen, so SenA-CM group was to simulate the Sennoside A metabolic mixture *in vitro* (Experiment 1). To rule out the effect of normal fecal supernatant on the growth of *A. muciniphila*, the fecal supernatant was set up as a control group (Experiment 2). Rhein, an important end product of Sennoside A subjected to β-glucosidase hydrolysis was evaluated simultaneously (Experiment 3) [15]. There was nosignificant difference between Sen-CM and Ctrl-CM group on the growth of *A. muciniphila* at different time points (**Figure 2F)**. Sennoside A and rhein both had not effect on the growth of *A. muciniphila* at different time points. Altogether, the dominant growth of *A. muciniphila* was not directly induced by sennoside A and its metabolites.

Result 3Sennoside A–mediateddecrement of *Clostridiales* causes butyrate reduction.

Further genus-level STAMP difference analysis (Welch's *t*-test, $P<0.05$) was performed [21]. Sennoside A-elevated species (*Akkermansia* and *Sutterella*) were consistent with biomarkers derived from LEfSe analysis whereas the suppressor spp. *Coprcoccus*, *Prevotella*, *Oscillospira*, *Ruminococcus* mainly involved in dietary fiber metabolism to synthesize SCFAs (**Figure S4 and Table S1**). An order level analysis pointed out that sennoside A significantly inhibited the relative abundance of *Clostridiales* (**Figure 3A**), which were the most predominant butyrate-producing taxon. Considering the dominant growth of *A. muciniphila* was identified on the 56th day of continuous sennoseide A treatment and sennoside A had no direct effect for *A. muciniphila in vitro*, we further observed the dynamic effects of sennoside A on *Clostridiales*. As **Figure 3B** below, the significant inhibitory effect of sennoside A on *Clostridiales* growth occurred at 28 days, earlier than the time of *A. muciniphila* dominant growth. Based on this speculation, sennoside A was superior to promote *A. muciniphila* growth, which was a secondary effect of its growth inhibition on *Clostridiales*.

To ask whether sennoside A is more effective on *Clostridiales* growth and has a direct inhibitory effect, we further performed an *in vitro* growth assay by selecting two major Clostridium butyricum producing species - i.e. *Clostridium tyrobutyrate* and *Clostridium butyricum*. Results as shown in **Figure 3D&E**,

sennoside A prototype had little effect on the growth of *C. butyricum* and *C. tyrobutyrate* without statistical significance. SenA-CM began to significantly inhibit at a concentration of 6.25% after 24 hours of administration ofsennoside A metabolites *C. butyricum* (24 h; 6.25% SenA-CM *v.s* 6.25% Ctrl-CM, **P*<0.05), which could be significantly inhibited at 50% concentration of the growth of *C. tyrobutyrate* (24 h; 50% SenA-CM *v.s* 50% Ctrl-CM, ***P*<0.01). In addition, rhein, the major metabolite of sennoside A, significantly inhibited the growth of *C. butyricum* at 0.5 *μ*M at 24 hours (24 h; 0.5 *μ*M *v.s* 0 *μ*M, ##*P*<0.01), which was significantly inhibited *C. tyrobutyrate* at 2 μM (24 h; 2 μM *v.s* 0 μM, #*P*<0.01). After 48 hours of exposure, the inhibition efficacy of SenA-CM with Rhein on the growth of *C. butyricum* and *C. tyrobutyrate* decreased. SenA-CM required up to 50% concentration to produce significant inhibition to *C. butyricum* and *C. tyrobutyrate*. And the potency of Rhein on *C. butyricum* and *C. tyrobutyrate* has also increased. In this study, we found that sennoside A can directly inhibit clostridium in the intestine, which was not mediated by its prototype, but of the primary metabolite rhein.

Next, short-chain fatty acid levels SCFAs were quantified to verify that microbial fiber metabolism was disrupted by sennoside A. We observed significantly lower concentrations of the SCFAs butyrate, as well as valeric acid and isovalerate in mice treated with sennoside A (**Figure 3D and Figure S5**), which were consistent with the decreased abundance of butyric-producing bacteria. Overall, sennoside A may decrease the abundance of butyric-producing bacteria by affecting intestinal bacterial community structure, and thus reducing the content of intestinal butyric acid.

Result 4 Sennoside A-induced intestinal microbial disturbance is a key step to intestinal mucosal barrier function damage

To elucidate whether intestinal bacterial homeostasis is causal for sennoside A-generated damage to the colonic mucus barrier, we performed fecal bacteria transplantation experiment. After initial antibiotic cocktail treatment, mice received a weekly microbial transplant from the sennoside A group (SenA-ABX) and Ctrl group (Ctrl-ABX) (**Figure 4A**). We observed that colonic mucus layer thickness and goblet cell number were significantly inhibited in SenA-ABX mice in comparison with Ctrl-ABX mice (**Figure 4B**). Live-imaging of FD4-gavaged mice revealed that fecal bacteria derived from sennoside A group resulted in the disruption of intestinal barrier function integrity with a diffuse-like distribution in the abdominal cavity. Moreover, FD4 leaked into colonic epithelial tissue, and the content of FD4 in serum increased (**Figure 4C&D**). In addition, fecal bacteria transplantation after sennoside A (100 mg/kg) treatment could significantly promote the translocation of intraluminal microorganisms into colonic epithelial tissue (**Figure 4E&F**).

To determine whether short-chain fatty acid content were closely related to the alterations in intestinal bacteria affected by sennoside A, we further examined potential reduction in the content of multiple short-chain fatty acids. As a result, consistent with animals chronically treated with Sennoside A, fecal bacteria transplantation derived from the sennoside A group did not affect changes in acetic acid content, but decreased valeric and butyric acid content compared with the Ctrl and Ctrl-ABX groups (**Figure 4G**). The results showed that the change of short-chain fatty acid content such as butyric acid by sennoside A was

closely related to its effect on intestinal bacteria. Further analysis of the bacterial community structure, as shown in **Figure S6A-E**, sennoside A (100 mg/kg) fecal bacteria transplantation group (SenA-ABX) and Sennoside A (100 mg/kg, SenA) group had lower α-diversity than control group (**Figure S6F**). The results of β-diversity analysis (PcoA, Weighted Unidrac) showed that the composition of SenA-ABX bacteria was similar to that of SenA for a long time, and significantly grouped with that of Control group bacteria (**Figure 4H**).

Result 5 Butyrate partially shapes gut dysbiosis and ameliorates intestinal epithelial barrier impairment in sennoside A-treated mice

The short-chain fatty acids butyrate, acetate and propionate are the major end products of dietary fiber, which provide approximately 10% of the calories we absorb [22]. Mucin O-glycans serve as an endogenous fermentation substrate for butyrate production [23]. Based on the aforementioned results, we hypothesized that the lower of butyrate triggered by the decrease of butyrate-producing bacteria may be the reason for the increase of *A. muciniphila.* Since the abundance of *Clostridiales* was dramatically reduced after 28 and 42 days of sennoside A treated, we thus treated mice with Sennoside A for 4 weeks and supplemented their drinking water with 150 mM sodium butyrate (Bt-SenA) [24,25] (**Figure 5A**). Consequently, the microbial structures in sennoside A-treated mice with sodium butyrate were different from those in sennoside A mice, but the microbial alpha-diversity was no affected (**Figure S7A&B**). The *Clostridiales* was the hallmark bacterium of Bt-SenA group rather than *A. muciniphila* (**Figure 5B and Figure S7C**), and the relative abundance of *Clostridiales* was significantly increased. (**Figure S7D**).

We next tested whether oral administration of sodium butyrate prevented sennoside A-induced intestinal epithelial barrier impairment in C57BL/6 mice. In line with our expectations, the mucosal barrier damage phenotype in the mucous layer, permeability, bacteria translocation and mechanical barrier were alleviated in sennoside A-treated mice (**Figure 5C-G and Figure S8**).

Result 6 Sennoside A induces low-grade inflammation as well as metabolic disorders

When the intestinal barrier is damaged, intestinal barrier permeability increases and mucus secretion decreases, bacteria and their secreted metabolites are with a higher probability of direct contact with epithelial cells, invading the mucosal layer, and activating the body's immune response [26,27]. After sennoside A treatment, body weight and the epididymis adipose mass significantly reduced, which might be related to its purgative and weight-loss efficacy **(Figure 6A and Figure S9A).** In addition, we found that sennoside A was able to significantly reduce colon length, which was nearly comparable to the colon length of mice in the DSS chronic colon inflammation model group (**Figure 6B**). To determine whether sennoside A could induce low-level inflammation, we examined fecal lipocalin (LCN2), a neutrophil protein that binds bacterial siderophores and is a sensitive and broadly dynamic marker of low-grade inflammation in mice [28]. Faecal LCN2 levels was increased in the group of 50 mg/kg and 100 mg/kg of sennoside A treatment at 56 days. On day 84, 100 mg/kg Sennoside A caused a dramatic increase in LCN2 (approximately 10 to 15-fold *v.s* Ctrl) (**Figure 6C**.). By using luminex assay to detect ten inflammatory factors in mouse serum, we found that sennoside A was able to induce an increased level

of a variety of proinflammatory factors, including IFN-γ, MIP-2, IL-17 as well as GM-CSF (**Figure 6D**). Further examination of the number of Th1, Th2, and Th17 cells in mesenteric lymph nodes revealed that sennoside A resulted in a significant increase proportion of Th1 cells as well as Th17 cells, but not Th2 cells (**Figure 6E&F and Figure S9C**). The increase of Th17 cells is also consistent with the decline of butyrate, due to the ability of butyrate to activate GPR109a thereby inhibiting Th17 cells [29]. Although sennoside A does not cause active colitis, low-grade intestinal inflammation induced by Sennoside A is associated with increased incidence of colon cancer[28,30]. Proliferation of epithelial cells, measured by Ki67 expression, was already significantly increased in sennoside A-treated mice which was ameliorated by sodium butyrate (**Figure S10**). The above results demonstrate that long-term sennoside A treatment induces chronic low-grade Inflammation.

Metabolic disorders is associated with, and defined by elevated by chronic low-grade inflammation, which also is capable of affecting the incidence of colon cancer [31,32]. To assess metabolic alternations in response to microbial dysbiosis and low-grade inflammation by sennoside A, untargeted metabolome profiles were generated on feces samples. Distinct clustering of metabolites was apparent between control and sennoside A-treated mice groups by principal components analysis model with distinct separation of two groups **(Figure7A)**. Sennoside A-treatment was sufficient to trigger widespread changes of metabolites, and obtained 50 differential metabolites based on fold change greater than 2 and *P* value less than 0.05 (**Figure S11 and supplementary dataset S1**). The topology map generated by MetaboAnalyst (www.metaboanalyst.ca) described the impact of sennoside A on these responsive metabolites and revealed the most significant pathways including purine metabolism, Pantothenate and CoA biosynthesis, beta–Alanine metabolism, Arginine biosynthesis, Butanoate metabolism, and so on (**Figure 7B**). The levels of thymine, xanthosine, creatinine, orotic acid were significantly elevated in feces of sennoside A groups compared to control mice which are key nodes of altered metabolic pathway (**Figure 7C**).

Result 7 Sennoside A exacerbates carcinogenesis in a colitis-associated cancer model

Using the azoxymethane (AOM)/DSS chemical-induced colon cancer model, we evaluated the effect of sennoside A on advancement of colon cancer. As shown in **Figure 8A&B**, colon length and body weight were significantly reduced in the AOM/DSS and AOM/DSS/Sennoside A groups compared with the control group, while there was no significant difference between the two groups. Notably, colonic adenomas were already evident in the AOM/DSS/Sennoside A group at the time for 40 days treatment, while only a few adenomas were produced in the AOM/DSS group animals. Besides, the tumor volume in the sennoside A-treated group was significantly increased compared with the AOM/DSS group, indicating that sennoside A already with a certain promoting effect on the occurrence of colon tumors at 40 days (**Figure 8C&D**). After sacrificed the animal at day 90, we found that the number and size of colonic adenomas were significantly increased in the presence of sennoside A. Although adenomas had also formed in the AOM/DSS group, sennoside A significantly promoted the development and progression of colonic tumors. Furthermore, we found soaring of LCN2 in feces in the AOM/DSS as well as AOM/DSS/Sennoside A groups at day 40. AOM/DSS/Sennoside A group had a tendency to increase

LCN2 levels compared with AOM/DSS at the same time point of AOM/DSS/Sennoside A group showing an increase in the number of tumors, suggesting that the low level of inflammation caused by sennoside A may promote tumor formation. LCN2 content tended to be similar in both groups at 90 days, which was possibly due to increased inflammation caused by long-term DSS consumption, thus the low-level inflammatory effect caused by sennoside A was weakened and could not be reflected as an accurate indicator (**Figure 8E&F**). Increased Th17 cell infiltration in mesenteric lymph nodes and increased IL-17 secretion in serum suggest that it may increase the phosphorylation level of STAT3 by activating JAK2/STAT3 signaling pathway, thereby activating the transcription of downstream genes related to cell survival such as BCL2, BAX, and BCL2L1, conferring the cells in an overactive proliferative state[24,25]. As Shown in **Figure 8G**, we found that the AOM/DSS/Sennoside A group had significantly higher levels of p-Stat3 than the AOM/DSS group. Besides, Wnt/β-catenin plays an important role in cell proliferation as well as tumorigenesis, and downstream target genes of β-cateninsuch as *Myc* and *Ccnd1*, can also promote the proliferation level of cells [33,34]. **Figure 8G** also exhibited that sennoside A remarkably upregulated the expression level of β-catenin. By examining the proliferation levels of tissues adjacent to colon tumors we found that sennoside A resulted in an increase in the level of epithelial cell proliferation near the tumor tissue, suggesting a possible malignant proliferative transition of epithelial cells (**Figure 8H**). Collectively, our data demonstrate that sennoside A has tumor-promoting effect in colitis-associated colonic carcinoma,

Discussion

Anthraquinone laxatives (i.e., Senna) and purgative botanicals (rhubarb, aloe vera, Senna, *etc*) containing anthraquinone compounds are used frequently in clinic, but the possible risk of anthraquinone use for the development of colorectal neoplasms has been controversial for a long time [3, 4, 7]. Previous studies with sporadic experimental data indicate that anthraquinone compound causes damage to the structure of colonic epithelial tissue. Prospective study data also indicate that long-term anthraquinone-use has a certain correlation with colon cancer development. However, limited evidence cannot positively interpret the potential adverse effects of anthraquinone laxatives. In this study, we innovatively paid attention to the integrity of the intestinal mucosal barrier, the first line of defense against commensal microorganisms and invading pathogens. We observed that sennoside A can disrupt the intestinal mucosal barrier by disrupting the homeostasis of intestinal bacteria and cause the production of intestinal epithelial inflammation, thereby promoting the development of colon cancer. Starting from the key initial link in the occurrence of colon cancer, microbiota-mediated mechanisms that connect long-term intake of anthraquinone laxatives to the progress of gastrointestinal inflammation and cancer have not been described.

The integrity of the intestinal mucosal barrier is the key start in the development of colon cancer in intestinal microbiota-mediated colitis. The intestinal mucosal barrier is usually divided into four barrier systems, including mechanical barrier, chemical barrier, microbial barrier and immune barrier [35]. All colonic pathologies arise from damage to the physical barrier (mechanical barrier and mucus layer in the chemical barrier), of which, the mucus layer is the first line of defense to insulate the intraluminal

microbiota from direct contact with colonic epithelial tissue. Microorganisms are in direct contact with the colonic epithelial tissue when the first line of defense is breached, so that promoting the increase of colonic permeability, bacterial translocation to the epithelial layer, and further inducing colonic inflammation and metabolic disorders. Long-term low-grade recurrent inflammation can activate cancer-promoting signaling axes such as STAT3 and β-Catenin, further promoting the development of colon cancer[36, 37].

Here, we have shown that long-term (84 days) administration of sennoside A (50, 100 mg/kg) can promote the changes in the structure and morphology of colonic crypts, promote the expression and distribution of tight junction protein (ZO-1, claudin-1) and adhesion protein (E-cadherin) in colonic epithelial tissues, but not directly induce the damage to the colonic epithelial cells. Consistently, sennoside A induces damage to the physical barrier of the colon, disrupts colonic barrier function and promotes increased colonic permeability as well as bacterial translocation to the colonic epithelium.

Given the role of gut microbes in the colonic mucosal barrier cannot be ignored, we set up to examine the effect of Sennoside A on gut microbial community structure. Sennoside A significantly promoted the dominant abundance of Verrucomicrobia phyla, and significantly inhibited the relative abundance of Firmicutes. Lefse analysis showed that *A. muciniphila* is the hallmark biomarker of the Sennoside (100 mg/kg) group. *A. muciniphila* is a key specie of the mucosymbiotic microbiome, a class of exclusive mucin-degrading bacteria that depends and only relies on mucins as the sole carbon source. Therefore, it may be reasonable to cause the damage to the integrity of the mucus barrier “wall” and the “channel” for microbial translocation to epithelial tissues. Sennoside A promotes the dominant growth of *Akkermansia muciniphila*, which disrupts the dynamic balance of colonic mucus synthesis and degradation. Considering the sensitivity of dynamic alterations in gut microbiome composition, fecal microbial community dynamics show that it is an incremental process of dominant growth in *A. muciniphila* by sennoside A. At the early stage of sennoside A administration, there were no significant effect on the relative abundance of *A. muciniphila*, but began to show significant growth promoting effect after 56 days of continuous gavage. Does Sennoside A directly promote the growth of A. muciniphila? Further *in vitro* flora culture confirmed that the prototype of Sennoside A, the metabolic mixture of Sennoside A and the main metabolite Rhein had no significant effect on the growth of *A. muciniphila*.

In addition, the growth inhibition of several SCFA-producing genuse by sennoside A, especially butyrate producing bacteria, is earlier than the promotion of *A. muciniphila* dominant growth. Butyrate is the preferred energy source for colonocytes and is locally consumed [37]. Acetate production by *Akkermansia muciniphila* also serve as energy substrates [38]. Presumably, the promotion of sennoside A on *A. muciniphila* is a secondary reaction of its growth inhibition on *Clostridiales* in consideration of the energy source for colonocytes in the absence of butyric acid. Further investigation of the direct bacteriostatic effect of Sennoside A *in vitro* by two major butyric acid-producing bacteria (*Clostridium tyrobutyrate* and *Clostridium butyricum*) showed that Sennoside A in the intestine could directly inhibit the growth of *C. tyrobutyrate* and *C. butyricum* by unchanged sennoside A, but by a direct bacteriostatic effect produced by its metabolites, especially rhein. Consistent with the microbiota analysis data, the decrease in the

abundance of butyrogenic bacteria resulted in a decrease of butyric acid levels. Butyrate absence also leads to impairment of intestinal barrier function. To clarify whether the disturbance of the microbiota caused by sennoside A is the key of the degradation of mucin and the disruption of intestinal mucosal barrier, the study evaluated the contribution of intestinal microorganisms in this process by fecal microbiota transplantation (FMT). Furthermore, butyrate exerts protective effects on intestinal homeostasis and intestinal barrier function. These findings provide strong evidence that intestinal microorganisms and their metabolites of sennoside A are involved in destabilized intestinal mucosal barrier integrity.

Sinve sennoside A induces the advance of low-grade inflammation in the colon, is there a link between butyrate loss and inflammation? To this end, the secretion of various inflammatory factors in the serum of mice was detected using a liquid chip, and we found that sennoside A can induce an increase in the levels of various proinflammatory factors such as the low-level inflammatory marker LCN2 and IL-17, IFN-γ, and MIP-2, and an increase in the number of Th1 and Th17 cells, further indicating the low-level inflammation caused by sennoside A. The present work highlights that low-grade inflammation can also agitate metabolic disorders in the body and contribute to the development of a variety of diseases [39, 40]. Based on metabolomics studies, sennoside A is found to cause metabolic abnormalities, including purine metabolism, pyrimidine metabolism and a variety of amino acid metabolism. Our results shed that a long-time state of low level inflammation is responsible for probability of colon tumors. Taken together, we speculated that sennoside A may not lead to tumorigenesis in a delayed manner, and its effect on the low level of inflammation caused by intestinal bacteria may be able to promote the development of colon cancer.

Sennoside A alone did not induce colonic inflammation as well as adenoma development. However, we observed typical changes featured by the chronic low-level inflammation state induced by Sennoside A, which might accelerate the development of colon tumors [1]. Further studies with the AOM/DSS chemical-induced carcinogenesis model found that sennoside A promoted the occurrence and development of colon cancer. AOM/DSS mice treated with sennoside A developed tumors earlier than control mice, and AOM/DSS model applied to C57BL/6 mice usually required three rounds (about 60 days) of DSS induction to form colonic adenomas. Significantly, sennoside A shortened the process. At the end of the experiment (90 days), we also found an increase of tumor number and size, accompanied by a more intense activation of STAT3and β-catenin signaling pathways, and promoted the proliferation of epithelial cells near the tumor, suggesting a possible malignant transition. At 40 days, tumor occurrence and volume were correspondingly increased, indicating that the low-grade inflammatory process in the colon was activated by sennoside A, which was consistent with previous studies on the carcinogenic effect of sennoside A.

Conclusion

In summary, our results provide evidence for the inflammatory carcinogenic risk of sennoside A, a representative component of anthraquinone laxatives. Sennoside A induced the decrease in butyric-

producing bacteria and consequently increased the growth of *A. muciniphila*, which disrupted the intestinal mucosal barrier function, initiated the low-grade inflammation and metabolic disorders, and ultimately promoted the development of colon tumors (Fig. 9**)**. Our study emphasizes that sennoside A promotes progression of colon cancer by disrupting the balance between mucus-degrading bacteria and butyrate-producing bacteria and impairing intestinal mucosal barrier integrity to induce colonic inflammation production.

Materials And Methods

Drug administration and Animal experiments

Sennoside A (CAS. 81-27-6; HPLC 98.58%; store at 2-8℃) studied in this article were purchased from Biopuify Phytochemicals Ltd., China.

Animal experiments were conducted in accordance with the Institutional Animal Care and Use Committees of Nanjing University of Chinese medicine and followed guidelines issued by the National Institutes of Health. Six-week-old C57BL/6J male mice (18 to 20 g) were purchased from the Model Animal Research Center of Nanjing University (Nanjing, China). Mice were housed under standard laboratory conditions (room temperature: (22±2) ℃; humidity: (50±5) %) with a light/dark cycle of 12/12 h. Before the experiment, they were acclimatized to the environment with free access to food and water for at least 3 days.

Animal protocol 1: Effects of Sennoside A on direct effect in mice

Mice were randomly distributed and plus daily administration of Sennoside A at 0, 25, 50, or 100 mg/kg by intragastric gavage for 12 weeks. Faecal sample from each group was collected weekly and stored at -80°C. Abundances were averaged across time points as shown in Figure 2&3. At the end of the experiment, the mice were sacrificed, and the blood and colon tissues were collected for analysis.

Animal protocol 2: Antibiotic treatment and fecal microbiota transplantation

For *in vivo* antibiotic protreatment, six-week-old male C57BL/6 J mice were supplemented with antibiotics vancomycin (0.5 g/liter), neomycin sulfate (1 g/liter), metronidazole (1 g/liter), and ampicillin (1 g/liter) in drinking water for five days.

After antibiotic treatment, fecal transplant was performed on the basis of an established protocol [41]. Briefly, 6-week-old male donor mice were given NS and Sennoside A (100mg/kg) for 12 weeks. During week 10 to week 12 (total of 14 days), faecal microbiota from each donor mouse was collected daily and stored at −80°C. The stools from donor mice of each group were pooled and 150–180 mg was resuspended in 1 ml of sterile saline. The solution was vigorously mixed for 10 s using a benchtop vortex (MS 3, IKA, Germany), and centrifuged at 800 g for 3 min. The supernatant was collected and used as transplant material as described below. Fresh transplant material was prepared on the same day of transplantation within 10 min before oral gavage to prevent changes in bacterial composition. Before

being killed for subsequent analysis, six-week-old male recipient mice were inoculated weekly with fresh transplant material (100 µl for each mouse) by oral gavage for 12 weeks. (**Figure 4**)

Animal protocol 3: Butyrate supplement in Sennoside A-treated mice.

Mice were maintained on Sennoside A-treatment for four weeks and divided into two subgroups (10 mice/group). Two groups continued to be treated with Sennoside A and simultaneously drinked with 150 mM sodium butyrate or placebo for the last eight weeks according to our microbiota analysis of compositional dynamics, respectively.

Animal protocol 4: The effect of sennoside A on AOM/DSS-induced colon cancer in mice.

C57BL/6 male mice (age, 6 weeks) were treated daily with Sennoside A (100mg/kg) or saline by oral gavage throughout the experiment. After 1 week on intraperitoneal injection with AOM (10 mg/kg; Sigma-Aldrich), the mice were given 1.5% DSS in drinking water for 5 days followed by regular drinking water for 10 days. This cycle was repeated for three times and the mice were sacrificed for analysis of colon tumorigenesis at day 40 and 90 after the AOM injection.

Haematoxylin and eosin staining and histopathologic analysis

Fresh intestinal mouse tissue was fixed in Carnoy's fixative solution (60% methanol, 30% chloroform, 10% glacial acetic acid) for at least 24 hours and processed into paraffin-embedded tissue sections. Post Carnoy's fixation, tissues were sectioned at 5 µm thickness using standard protocols. To determine the extent of the damage, the H&E-stained slides were scored on a scale of 0-3 for four parameters: 3=markedly increased, 2=moderately increased, 1=slightly increased and 0=normal. The scoring parameters were the amount of crypt atrophy (including the number and depth of crypt), polymorphonuclear leukocyte infiltrate in crypt, the counts of goblet cells per crypt, Lymphocyte of basement of crypt and mucous membrane base.

The colonic mucus layer measurements

To measure the thickness of the colonic inner mucus layer, colonic tissues were sectioned at 5µm thickness, deparaffinized and stained using Alcian Blue staining kit (Leagene, Beijing, China) and anti-Muc2 (sc-515032, Santa cruz Biotechnology) immunofluorescent staining according to the manufacturer's instructions.

Measurement of intestinal permeability with FITC-Dextran

Fluorescence detection in living, anesthetized mice was captured with a IVIS™ liveimaging system (IVIS Lumina III, PerkinElmer). Mice were gavaged with fluorescein-isothiocyanate (FITC)-dextran (4kDa; Sigma) at a doseage of 400mg/kg and then animals were studied 1 hr later using multispectral fluorescent capture. Blood samples were obtained after 4-5hr by retro-orbital bleeding, and the fluorescence intensity in the serum was measured at an excitation wavelength of 485 nm and an

emission wavelength of 520 nm using a Microplate System (EnSpire, Perkin Elmer). FITC-dextran diluted in PBS was used to plot a standard curve, and the serum concentration of FITC-dextran was calculated. Furthermore, the mouse ileal-tissue sections were fixed with Carnoy's fluid and thin sections (~5 mm) were cut and deposited on glass slides. Images were acquired using Inverted fluorescence Microscope (Alexa Fluor 488, Axio vert A1, ZEISS).

Analysis of tight-junction proteins

The tissue sections and NCM-460 cell were immunostained with specific antibodies (claudin-1 (A-9) (mouse) Santa cruz sc-166338; ZO-1 (D6L1E) Rabbit mAb CST 13663 ; E-Cadherin (4A2) Mouse mAb, CST 14472) by incubating overnight at 4℃. Following antibody incubation, slides were incubated with Alexa Fluor 594 or 488 -conjugated secondary antibody for 2 hr at room temperature followed by washing three times with PBS (3 cycles, 5 min). The nuclei were stained with DAPI and slides were mounted in ProLong antifade reagent. Markings were detected and photographed by Inverted fluorescence Microscope (Axio vert A1, ZEISS).

To extract proteins from ileal epithelial cells, the epithelial cell fraction from ileal tissues were isolated. Total protein lysates were fractionate d by 10% SDS-PAGE and electro-blotted onto polyvinylidene difluoride membranes (Immobilon TM-P; Millipore, USA). Afterwards, the membranes were blocked with 5% non-fat milk for 1 h at room temperature in TBST buffer (10 mM Tris, 150 mM NaCl, pH 7.6, 0.1% Tween 20) and probed with primary antibodies overnight at 4°C. The membranes were then incubated with horseradish peroxidase-conjugated secondary antibody. The dilutions of primary and secondary antibodies have been described in the Antibody subsection above. Protein bands were developed using enhanced chemiluminescence reagent (Millipore). The blots were probed with the primary antibodies against GAPDH (Bioworld, China), claudin-1, ZO-1 and E-Cadherin (instrument same as above).

Bacterial Translocation by Fluorescent in situ hybridization (FISH)

Mucus immunostaining was paired with fluorescent *in situ* hybridization (FISH), as previously described [42], in order to analyze bacteria localization at the surface of the intestinal mucosa. Five-µm sections were cut and dewaxed by preheating at 60℃ for 10min, followed by bathing in xylene at 60℃ for 10 min, xylene at room temperature for 10min and 99.5% ethanol for 10min. After deparaniffization and rehydratation, sections were incubated in hybridization buffer [20 mM Tris-HCl, 0.9 M NaCl and 0.1% SDS (pH 7.2)] 10 min at 50℃. Next, sections were incubated with 100 nM EUB338I probe (Sequence 5’-GCT GCCTCC CGT AGG AGT-3’, FITC-conjugated, FB-0010B, EXONBIO) in hybridization buffer in the dark, overnight at 42℃ . After washing for 10min in wash buffer (20mM Tris-HCl, pH7.4, 0.9M NaCl) and 3×10min in PBS, Mucin 2 primary antibody was diluted to 1:200 in block solution and applied overnight at 4℃. After washing in PBS, block solution containing anti-mouse Alexa 594 secondary antibody (A-21203, Invitrogen) and Hoechst 33258 was applied to the section for 3h. Observations were performed with a Zeiss-Axio vert A1 microscope. The distance between bacterial populations and the epithelial surface was measured at four points of the proximal, middle and distal colon in each mouse.

Gut Microbiota Analysis by 16S Sequencing

Stool samples (n=5 per group) were snap-frozen in liquid nitrogen before storage at -80°C. Total genomic DNA was extracted from samples using the CTAB/SDS method. DNA concentration and purity were monitored on 1% agarose gel. According to the concentration, DNA was diluted to 1 ng/μl using sterile water. 16S rRNA genes were amplified using specific primer with the barcode. All PCR reactions were carried out in a 30 μL system comprising 15 μL of Phusion High-Fidelity PCR Master Mix (New England Biolabs), 0.2 μM of forward and reverse primers, and about 10 ng template DNA. The thermal cycling consisted of initial denaturation at 95°C for 3 min, followed by 25 cycles of denaturation at 95°C for 30 s, annealing at 55°C for 30 s, and elongation at 72°C for 30 s, and finally at 16°C for 2 min. The V3 and V4 hypervariable regions of the 16sRNA gene were amplified. The same volumes of 1´ loading buffer (containing SYB green) and PCR products were mixed, and electrophoresis was performed on 2% agarose gel. Samples with bright main strip between 460 bp (V3+V4) were chosen for further experiments. PCR products were mixed in equidensity ratios. Then, the mixture of PCR products was purified with GeneJET Gel Extraction Kit (Thermo Fisher Scientific, USA). Sequencing libraries were generated using NEB Next Ultra DNA Library Prep Kit for Illumina (NEB, USA) following manufacturer's recommendations and index codes were added. The library quality was assessed on Qubit@ 2.0 Fluorometer (Life Technologies, CA, USA) and Agilent Bioanalyzer 2100 system. At last, the library was sequenced on an Illumina MiSeq platform and 250 bp paired-end reads were generated.

Quality filtered reads were analyzed with the software package QIIME[43] High-quality reads for bioinformatics analysis were selected, and all of the valid reads from all samples were clustered into operational taxonomic units (OTUs) based on 97% sequence similarity. α-Diversity was calculated based on the Chao1 diversity index. The variation between the experimental groups (β-diversity) was assessed with principal coordinate analysis (PCoA) plots. Bacterial genuses with statistically significant difference were assessed using linear discriminant analysis effect size (LefSe) (http://huttenhower.sph.harvard.edu/galaxy)

Bacterial Growth Assays in corresponding treatment

Bacterial strains and culture conditions:

Akkermansia muciniphila , type strain, DMS 22959. The strain was cultured in 37℃,10% H2, 5% CO2 and 85% N2, medium 1203 +0.05% mucin

Clostridium tyrobutyrate, ATCC25755. The strain was cultured in 37℃, 0% H2, 5% CO2 and 85% N2, medium 2107

Clostridium butyricum, ATCC19398. The strain was cultured in 37℃, 0% H2, 5% CO2 and 85% N2, medium 2107

Experimental Design: A total of three in-vitro experiments (Experiments 1-3) were performed- details of the experimental replication are provided in the corresponding figure legends.

In-vitro Experiment 1, culture medium(CM) of bacterial growth condition was prepared in the following protocol: fresh faeces pellets from normal donor mice(50-100mg in 1ml PBS)→vortexing for 30min→ centrifuging 10min at 1000 g to remove faecal fibrous solids and collect bacteria-contained supernatants(500μl)→ supernatants supplemented LB medium(200μl) and treated with Sennoside A(1mg/ml)→ stationary incubation at 37°C for 4 hours under anaerobic atmosphere→centrifuging 10 min at 15000g to collect bacteria-free supernatants→ vacuum centrifugal concentration for ~8-12h→ resuspended in 1mL of corresponding strain medium (100%SenA-CM)→ A ten ponit concentration(%SenA-CM) using 2-fold serial dilutions was perpared.

In-vitro Experiment 2&3, all species were evaluated in different concentrations of compound prototypes (Sennoside A & Rhein).

All species were cultured in micro-anaerobic incubation system (ELECTROTEK, AW500SG/TG), and maintained at 37°C in a humidified incubator containing 10% H_2, 5% CO_2 and 85% N_2. Absorbance values were measured at 600nm (A600) at an interval of 12 hr over 36 hr except for *Akkermansia muciniphila*, for which the absorbance was measured over 72 hr, owing to its relatively slow growth.

Notes: The color of compounds (Sennoside A and Rhein) seriously affects the absorbance value of OD600. Therefore, the drug solution of different concentrations without bacteria (SenA, Sen A-CM, Rhein) was used as blank (see Table S1 for compositions of all growth media used in this study)

Quantification of Short-Chain Fatty Acids by GC-MS

Fecal samples stored at -80℃ were used to quantify short-chain fatty acids (SCFAs) including acetate, propionate, butyrate, valeric acid, isovalerate, and isobutyrate. Samples were first thawed on wet ice. Then, an equivalent amount of 0.05M NaOH was added (100 ul per 100 mg of material) to cecal contents (≥0.05 g) and the samples were thoroughly homogenized by vortexing for 20 min. Supernatants (500μl) were prepared by reconstituting all cecal content of each animal with 10μl of internal standard (d3-caproic acid, 500μg/ml), followed by centrifugation at 13000rpm for 10 min at 4°C. The mixture(supernatants-internal standard-NaOH) were kept on ice or frozen until quantification of SCFAs by GC-MS. The mixture was transferred to the glass tube, added with Milli-Q water and vortexed for 30 seconds. The SCFAs were extracted through the addition of 300 μL 1-propanol, 200μl pyridine and 150μl of propyl chlorocarbonate by vortex mixing for 1 min. After that, 500μl of hexyl hydride were added to the mixture, vortexed for 1min, and centrifuge at 3000rpm for 5min. The extracted samples were measured using a ISQ GC–MS (Thermo Fisher Scientific, Waltham, MA, USA) as described previously with a TR - SQC capillary column (15m× 0.25mm)).Helium was used as the carrier gas and injections(1 μl) were made in the split mode (10:1 split). Oven emperature was set at 50℃ and maintained for 10 min, raised to 70°C at 10°C/min, increased to 85°C at 3°C/min, elevated to 110℃ at 5°C/min, up to 290℃ at 30°C/min and held at this temperature for 8 min. Detector temperature was set at 290°C and the injector temperature was 260°C. SCFAs standards were mixtures of acetate, propionate, butyrate, isobutyrate, valerate, and isovalerate. All the Standards were purchased from Merck (Darmstadt, Germany).The

concentrations of SCFAs were calculated by the standard curve method. The reported values were normalized according to the wet weight of the original fecal sample used.

Metabolomics analysis.

For fecal metabolomics, approximate 50 mg fecal content for each mouse were collected at the end of experiment and added 0.8 ml ultrapure water containing 6 μg 1,2-$^{13}C_2$-myristic as an internal standard, vortex for 5 min, followed by centrifugation for 10 min at 13000 g. The supernatants were transferred to a new 1.5 ml tube. 400 μL of supernatants were dried in a SpeedVac sample concentrator and combined with 60 μL methoxyamine hydrochloride in pyridine (10mg/mL), then vortexed for 3 min and shaken at 30 °C for 90 min. 60 μL of BSTFA containing 1% TMCS were added to the sample and shaken at 30 °C for another 60 min. The mixture was then transferred to a sampler vial with a glass insert and subjected to GC–MS analysis. Quality control (QC) samples were prepared by pooling aliquots of all the fecal samples and were processed using same procedure as that for the experimental samples. Analysis was performed on a TRACE 1310 gas chromatograph equipped with an AS 1310 autosampler connected to a TSQ 8000 triple quadrupole mass spectrometer (Thermo Fisher Scientific, Waltham, MA, USA) as described previously[44]. Helium was used as the carrier gas, and was maintained at a constant flow of 1.2 mL/min. The oven temperature was initially maintained at 60 °C for 1 min, then increased to 320 °C at 20 °C/min, and then held constant for 5 min. The transfer line temperature between the gas chromatograph and the mass spectrometer was set to 250 °C. Electron impact ionization at 70 eV was employed, with an ion source temperature of 280 °C. Mass spectra were acquired with a scan range of 50–500 m/z and a time range of 3.5–19 min. Raw data were acquired from Xcalibur 2.2 software (Thermo Fisher Scientific) and metabolites were identified through matching of their mass spectra against the reference spectra in the NIST 2014 standard database built-in Xcalibur 2.2 software. Metabolic analyses were performed using MetaboAnalyst 4.0 (https://www.metaboanalyst.ca/). Differential metabolites were identified by fold change>2 and p value<0.05. Pathway enrichment analysis were carried out based on the above differential metabolites.

ELISA for Fecal Lipocalin

Frozen fecal samples (-80℃ stored) were used to determine the levels of fecal Lipocalin (LCN2). The assays were performed within 30 days of sample collection. The samples were prepared as mentioned previously[45], with a few modifications in the sample prepration protocol: fecal samples were thawed on wet ice and 40-70 mg of samples were separated in fresh tubes, to which 0.6 mL of 1% (v/v) Tween 20 (Sigma-Aldrich, USA) prepared in PBS was added. To get a homogeneous suspension, the samples were vortexed for 20 min. The suspension was then centrifuged at 4℃ for 10 min at 14000 rpm. Next, the supernatant was carefully recovered and stored at -20℃ until the analysis. To measure the LCN2 levels, a mouse Mouse Lipocalin-2/NGAL DuoSet ELISA (R&D systems, Cat.No.DY1857) was employed and the manufacturer's protocol was followed.

Measurement of cytokines in serum.

Cytokines and chemokines were measured a Luminex-100 system and the XMap Platform (Luminex Corporation). Each sample was run in duplicate in a 96-well micro titer plate using 25 µl serum using MILLIPLEX MAP Mouse Cytokine/Chemokine Magnetic Bead Panel (MCYTOMAG-70K-10, Millipore) containing KC, MIP-2, IFN-γ, IL-4, IL-6, GM-CSF, IL-1β, IL-17, IL-10 and TNF-α according to the manufacturer's instructions . Quality control of each sample was performed, and a bead count of < 50 was not used for analysis. The experimental design for the Luminex assay was carried out using PlateDesigner (platedesigner.net) with samples from the same patient being randomly allocated to a plate and well, guaranteeing that if technical confounders exist they can properly be adjusted for in the analysis steps[46].

Flow cytometry analysis.

Cells were isolated from mesenteric lymph nodes (mLNs) followed by tissue mashing through 100 µm cell strainers. Cells were counted and stimulated using Cell stimulation Cocktail plus transport inhibitors 500× (eBioscience cat. no. 00-4975-93) for 4 h in complete RPMI1640 containing 10% FBS. After stimulation, cells were harvested, fixed using IC fixation buffer and permeabilized using 1× permeabilization buffer (eBioscience). The following antibody clones were used: anti-CD3-APC (eBioscience, 17-0032-82), anti-CD4-FITC (eBioscience, cat. no. MA5-17443) and IL-17A-PerCP-Cyanine5.5 (eBioscience, 45-7177-82), IL-4-PE-Cy7 (8D4-8) (ebioscience, cat. no. 25-7049), IFN gamma PE(XMG1.2) (ebioscience, cat. no. 12-7311-82). Single cell suspensions were examined using BD Accuri C6 and the data were analyzed using C6 software and ata analyzed using FlowJo software.

Bacterial quantification by qPCR.

In addition to 16srDNA sequencing of the relative abundance of *Akkermansia muciniphila*, as a second approach to absolute quantification assay in fecal samples, phylotype-specific bacterial primers were designed. Total bacterial DNA was isolated from weighted faeces using E.Z.N.A Stool DNA KIT (Omega Bio-tek, USA). qPCR on a 7500 Sequence Detector (Applied Biosystems, CA, USA) was used to calculate the number of *A. municiphila*. DNA was then subjected to quantitative PCR using ChamQ SYBR qPCR Master Mix (Low ROX Premixed) (Vazyme, Shanghai, China) with following primers: Amuc_1599F (GACCGGCATGTTCAAGCAGACT) and Amuc_1599R (AAGCCGCATTGGGATTATTTGTT) to measure[45]. Standard curves for quantification consisted of ten-fold serial dilutions in the range of 108–101 copies of the 16S rRNA gene of the stool samples. Results are expressed as bacteria number per mg of stool, using a standard curve.

Statistical analysis

Unless otherwise stated in individual method sections above, statistical analysis was performed using GraphPad Prism V.7.0a. The results represent data from multiple independent experiments. Data were expressed as mean ± standard deviation (SD) or tandard error of the mean (SEM). The data were analyzed using two-tailed student's *t* test (for two groups) and one-way analysis of variance (ANOVA) (for

multiple groups). Statistically significancecewas shown with asterisks as follows: *p < 0.05, **p < 0.01, and ***p < 0.001.

Declarations

Ethics Committee Approval and Patient Consent

All experimental protocols were approved by the Animal Care and Use Committee of Nanjing University of Chinese Medicine (Nanjing, China) and conducted conforming to the Guidelines for the Care and Use of Laboratory Animals (ACU170904).

Consent for publication

Not applicable.

Data Availability

The datasets generated during and/or analyzed during the current study are available from the corresponding author on reasonable request.

Competing Interest

The authors declare that they have no competing interests

Funding

This work was financially supported by National Natural Science Foundation of China (81961128020, 81973734, 81673725, 81673795)

Authors' contributions

ZHW,JWW and YL designed the study protocol and supervised all parts of the project. PLS and YY conducted animal experiments. PC performed the molecular biology experiments. LT and YLS did the bioinformatics analyses in close collaboration with ZHW drafted the first versions. YLS and ZGS contributed to text revision and discussion. All authors read and approved the final manuscript.

Acknowledgements

The authors thank Prof. Jinjun Shan (Department of Pediatrics, Affiliated Hospital of Nanjing University of Chinese Medicine) for the quantification of Short-Chain Fatty Acids.

This project was supported in part by Jiangsu Province Traditional Chinese Medicine Leading Talents Program (SLJ0229).

References

1. Ford. Suares.Effect of laxatives and pharmacological therapies in chronic idiopathic constipation: systematic review and meta-analysis.Gut.2011; 60: 209–18.
2. Malik MüllerAnthraquinones. As Pharmacological Tools DrugsMed Res Rev. 2016;36:705–48.
3. Dufour G.Ultrastructure of mouse intestinal mucosa and changes observed after long term anthraquinone administration.Gut.1984; 25: 1358–63.
4. Mori S, Niwa Y, Tanaka. Hirono.Carcinogenicity of chrysazin in large intestine and liver of mice.Jpn. J Cancer Res. 1986;77:871–76.
5. Siegers, von, Otte. Schneider.Anthranoid laxative abuse–a risk for colorectal cancer.Gut.1993; 34: 1099–101.
6. Mereto, Ghia. Brambilla.Evaluation of the potential carcinogenic activity of Senna and Cascara glycosides for the rat colon. Cancer Lett. 1996;101:79–83.
7. NTP Toxicology and Carcinogenesis Studies of EMODIN (CAS NO. 518-82-1) Feed Studies in F344/N Rats and B6C3F1 Mice.Natl Toxicol Program Tech Rep Ser.2001; 493: 1–278.
8. Martens, Neumann. Desai.Interactions of commensal and pathogenic microorganisms with the intestinal mucosal barrier. Nat Rev Microbiol. 2018;16:457–70.
9. Cai, Cheng, Chen, Xu, Ding. Gu.Interactions of commensal and pathogenic microorganisms with the mucus layer in the colon.Gut Microbes.2020; 11: 680–90.
10. Abreu.Toll-like. receptor signalling in the intestinal epithelium: how bacterial recognition shapes intestinal function. Nat Rev Immunol. 2010;10:131–44.
11. Grivennikov W. Mucida, Stewart, Schnabl, Jauch, Taniguchi, Yu, Osterreicher, Hung, Datz, Feng, Fearon, Oukka, Tessarollo, Coppola, Yarovinsky, Cheroutre, Eckmann, Trinchieri, Karin.Adenoma-linked barrier defects and microbial products drive IL-23/IL-17-mediated tumour growth.Nature.2012; 491: 254–58.
12. Gallimore G. Epithelial barriers, microbiota, and colorectal cancer.N. Engl J Med. 2013;368:282–84.
13. Chen P. Wang.Microbiome, inflammation and colorectal cancer. Semin Immunol. 2017;32:43–53.
14. Li L. Fuhrer, Geuking, Lawson, Wyss, Brugiroux, Keller, Macpherson, Rupp, Stolp, Stein, Stecher, Sauer, McCoy, Macpherson.The outer mucus layer hosts a distinct intestinal microbial niche. Nat Commun. 2015;6:8292.
15. van Gorkom BA, de Vries EG, Karrenbeld. Kleibeuker.Review article: anthranoid laxatives and their potential carcinogenic effects.Aliment. Pharmacol Ther. 1999;13:443–52.
16. Van der Sluis M, De Koning BA, De Bruijn AC, Velcich, Meijerink, Van Goudoever JB, Büller, Dekker, Van Seuningen I, Renes. Einerhand.Muc2-deficient mice spontaneously develop colitis, indicating that MUC2 is critical for colonic protection.Gastroenterology.2006; 131: 117–29.
17. Schroeder GMH, Ståhlman, Arike MEV, Hansson. Bäckhed.Bifidobacteria or Fiber Protects against Diet-Induced Microbiota-Mediated Colonic Mucus Deterioration.Cell Host Microbe.2018; 23: 27–40.e7.

18. Wei Y. Rey, Ridaura, Davidson, Gordon, Semenkovich.Fatty acid synthase modulates intestinal barrier function through palmitoylation of mucin 2. Cell Host Microbe. 2012;11:140–52.
19. Okumura K, Nakano, Kayama, Kinoshita, Motooka. Gotoh, Kimura, Kamiyama, Kusu, Ueda, Wu, Iijima, Barman, Osawa, Matsuno, Nishimura, Ohba, Nakamura, Iida, Yamamoto, Umemoto, Sano, Takeda.Lypd8 promotes the segregation of flagellated microbiota and colonic epithelia.Nature.2016; 532: 117–21.
20. Tramontano A. Pruteanu, Klünemann, Kuhn, Galardini, Jouhten, Zelezniak, Zeller, Bork, Typas, Patil.Nutritional preferences of human gut bacteria reveal their metabolic idiosyncrasies.Nat Microbiol.2018; 3: 514–22.
21. Parks T. Hugenholtz, Beiko.STAMP: statistical analysis of taxonomic and functional profiles.Bioinformatics.2014; 30: 3123–24.
22. El A, Raoult G. Henrissat.The abundance and variety of carbohydrate-active enzymes in the human gut microbiota. Nat Rev Microbiol. 2013;11:497–504.
23. Yamada H. Iijima, Genda, Aoki, Nagata, Han, Hirota, Kinashi, Oguchi, Suda, Furusawa, Fujimura, Kunisawa, Hattori, Fukushima, Morita, Hase.Mucin O-glycans facilitate symbiosynthesis to maintain gut immune homeostasis.EBioMedicine.2019; 48: 513–25.
24. Li Y, Katiraei, Kooijman Z, Chung G, van den Heuvel JK, Meijer JFP, Heijink, Giera, van Dijk K. Groen, PCN, Wang.Butyrate reduces appetite and activates brown adipose tissue via the gut-brain neural circuit.Gut.2018; 67: 1269–79.
25. Fachi F, P, da, C, de Andrade, da Basso MCP, de Sales NOS, Souza E, Dos ÉL, Thomas SES, Setubal, Magalhães, Forti, Candreva, Rodrigues, de Jesus MB, Consonni ADS, Varga-Weisz, MAR.Butyrate Protects Mice from Clostridium difficile-Induced Colitis through an HIF-1-Dependent Mechanism.Cell Rep.2019; 27: 750 – 61.e7.
26. Yusung B. Molecular mimicry, inflammatory bowel disease, and the vaccine safety debate. BMC Med. 2014;12:166.
27. Brown R.Friends in Low Places: Intestinal Commensals Limit Colitis through Molecular Mimicry.Cell.2017; 171: 503–05.
28. Chassaing K. Goodrich, Poole, Srinivasan, Ley, Gewirtz.Dietary emulsifiers impact the mouse gut microbiota promoting colitis and metabolic syndrome.Nature.2015; 519: 92–96.
29. Koh, De Vadder F, Kovatcheva-Datchary. Bäckhed.From Dietary Fiber to Host Physiology: Short-Chain Fatty Acids as. Key Bacterial MetabolitesCell. 2016;165:1332–45.
30. Andrews. Gamache, Weingarten, Haimes.Intraspinal extension of an air cyst of the lung: case report.Neurosurgery.1989; 24: 414–17.
31. Manna T. Krausz, Haznadar, Xue, Matsubara, Bowman, Fearon, Harris, Shah, Gonzalez.Biomarkers of coordinate metabolic reprogramming in colorectal tumors in mice and humans.Gastroenterology.2014; 146: 1313–24.
32. Chassaing, Ley. Gewirtz.Intestinal epithelial cell toll-like receptor 5 regulates the intestinal microbiota to prevent low-grade inflammation and metabolic syndrome in mice.Gastroenterology.2014; 147:

1363-77.e17.

33. Arqués C. Puig, Tenbaum, Argilés, Dienstmann, Fernández, Caratù, Matito, Silberschmidt, Rodon, Landolfi, Prat, Espín, Charco, Nuciforo, Vivancos, Shao, Tabernero, Palmer.Tankyrase Inhibition Blocks Wnt/β-Catenin Pathway and Reverts Resistance to PI3K and AKT Inhibitors in the Treatment of Colorectal Cancer. Clin Cancer Res. 2016;22:644–56.
34. Tenbaum O-M. Puig, Chicote, Arqués, Landolfi, Fernández, Herance, Gispert, Mendizabal, Aguilar, Ramón, Schwartz, Vivancos, Espín, Rojas, Baselga, Tabernero, Muñoz, Palmer.β-catenin confers resistance to PI3K and AKT inhibitors and subverts FOXO3a to promote metastasis in colon cancer. Nat Med. 2012;18:892–901.
35. Sharkey, Beck. McKay.Neuroimmunophysiology of the gut: advances and emerging concepts focusing on the epithelium. Nat Rev Gastroenterol Hepatol. 2018;15:765–84.
36. Yu, Pardoll. Jove.STATs in cancer inflammation and immunity: a leading role for STAT3.Nat. Rev Cancer. 2009;9:798–809.
37. Dammann, Khare. Gasche.Tracing PAKs from GI inflammation to cancer.Gut.2014; 63: 1173–84.
38. Louis, Hold. Flint.The gut microbiota, bacterial metabolites and colorectal cancer.Nat. Rev Microbiol. 2014;12:661–72.
39. Khandekar, Cohen. Spiegelman.Molecular mechanisms of cancer development in obesity. Nat Rev Cancer. 2011;11:886–95.
40. Yu L. Herrmann, Buettner, Jove.Revisiting STAT3 signalling in cancer: new and unexpected biological functions. Nat Rev Cancer. 2014;14:736–46.
41. Li S, Li, Zhang, Cui, Yun, Yang, Zhang, Meng, Wu, Duan, Yang. Wu, Sun, Zou, Chen.Probiotics Ameliorate Colon Epithelial Injury Induced by Ambient Ultrafine Particles Exposure. Adv Sci (Weinh). 2019;6:1900972.
42. Johansson H.Preservation of mucus in histological sections, immunostaining of mucins in fixed tissue, and localization of bacteria with FISH.Methods Mol. Biol.2012; 842: 229–35.
43. Martinez D, Wahli. Mermod.Synergistic transcriptional activation by CTF/NF-I and the estrogen receptor involves stabilized interactions with a limiting target factor.Mol. Cell Biol. 1991;11:2937–45.
44. Li Y, Dai, Lin, Xie, He, Tao, Shan. Wang.Non-invasive urinary metabolomic profiles discriminate biliary atresia from infantile hepatitis syndrome.Metabolomics.2018; 14: 90.
45. Desai S. Koropatkin, Kamada, Hickey, Wolter, Pudlo, Kitamoto, Terrapon, Muller, Young, Henrissat, Wilmes, Stappenbeck, Núñez, Martens.A Dietary Fiber-Deprived Gut Microbiota Degrades the Colonic Mucus Barrier and Enhances Pathogen Susceptibility.Cell.2016; 167: 1339-53.e21.
46. Suprun. Suárez-Fariñas.PlateDesigner: a web-based application for the design of microplate experiments.Bioinformatics.2019; 35: 1605–07.

Figures

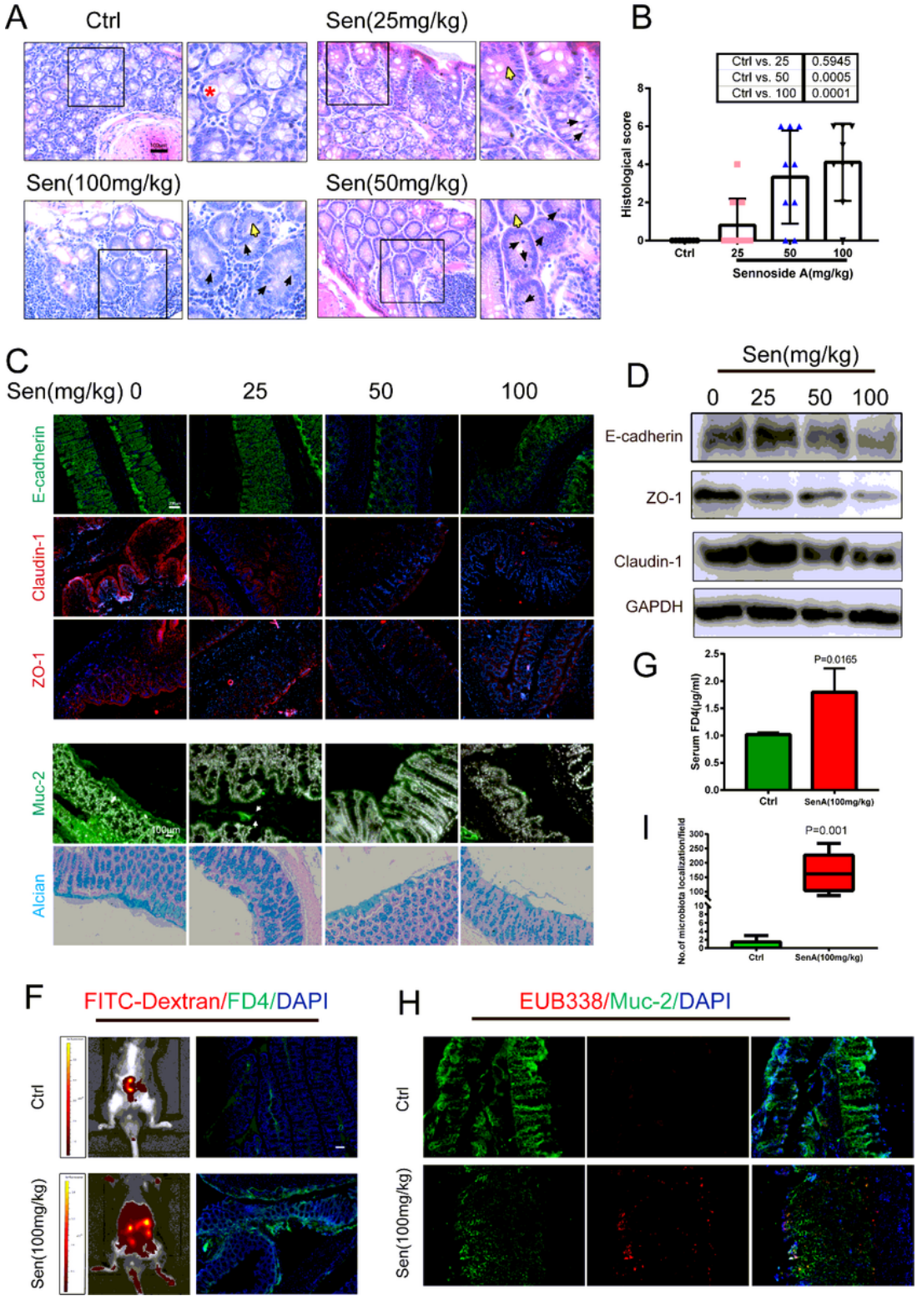

Figure 1

Sennoside A causes intestinal barrier injury and bacterial translocation. (A) Representative colon histological sections of sennoside A-treated mice and control mice (original magnification, ×400). Red asterisks mark goblet cells filled with mucus. Arrows indicate major histopathological differences between groups: polymorphonuclear infiltration of the crypt (black arrows), reduction of goblet cells (Yellow arrows). (B) Histological score of mice treated with sennoside A from colonic tissue sections (day

84). Each dot represents the histological score of one individual mouse. The horizontal bar represents the mean ± SD. (C) Images of the ileal villi sections showing the tight and adherens junction of claudin-1(red), E-cadherin (green), and ZO-1 (red) (magnification, ×200), as also seen in Figure S2. NCM-460 cell treatment with Sennoside A. (D) Immunoblot of cell-cell junction proteins claudin, E-cadherin and ZO-1 in whole- tissue lysates (H) of colon IECs. (E) Immunofluorescence images of colonic thin sections stained with a-Muc2 antibody and DAPI (magnification, ×400) and Alcian blue-stained colonic sections showing the inner mucus layer (magnification, ×200).Please note that the outer mucus layer is less defined and often not observed in fixed tissue sections.(F) In vivo detection of orally administered tracer (4-kDa FITC-dextran). Representative imaging of animal abdomen is shown on the left and fluorescence photography of the colonic epithelium on the right (magnification, ×100). (G) Quantitation of serum FD4 permeability. p=0.0165 (with data presented as mean ± SEM). (H) Microscopy analysis of microbiota localization: EUB338I probe (red), MuC-2 (green) and DAPI (blue). Magnification, ×100. (I) Number of bacterial localization in field.Data are mean ± SEM, P=0.01.

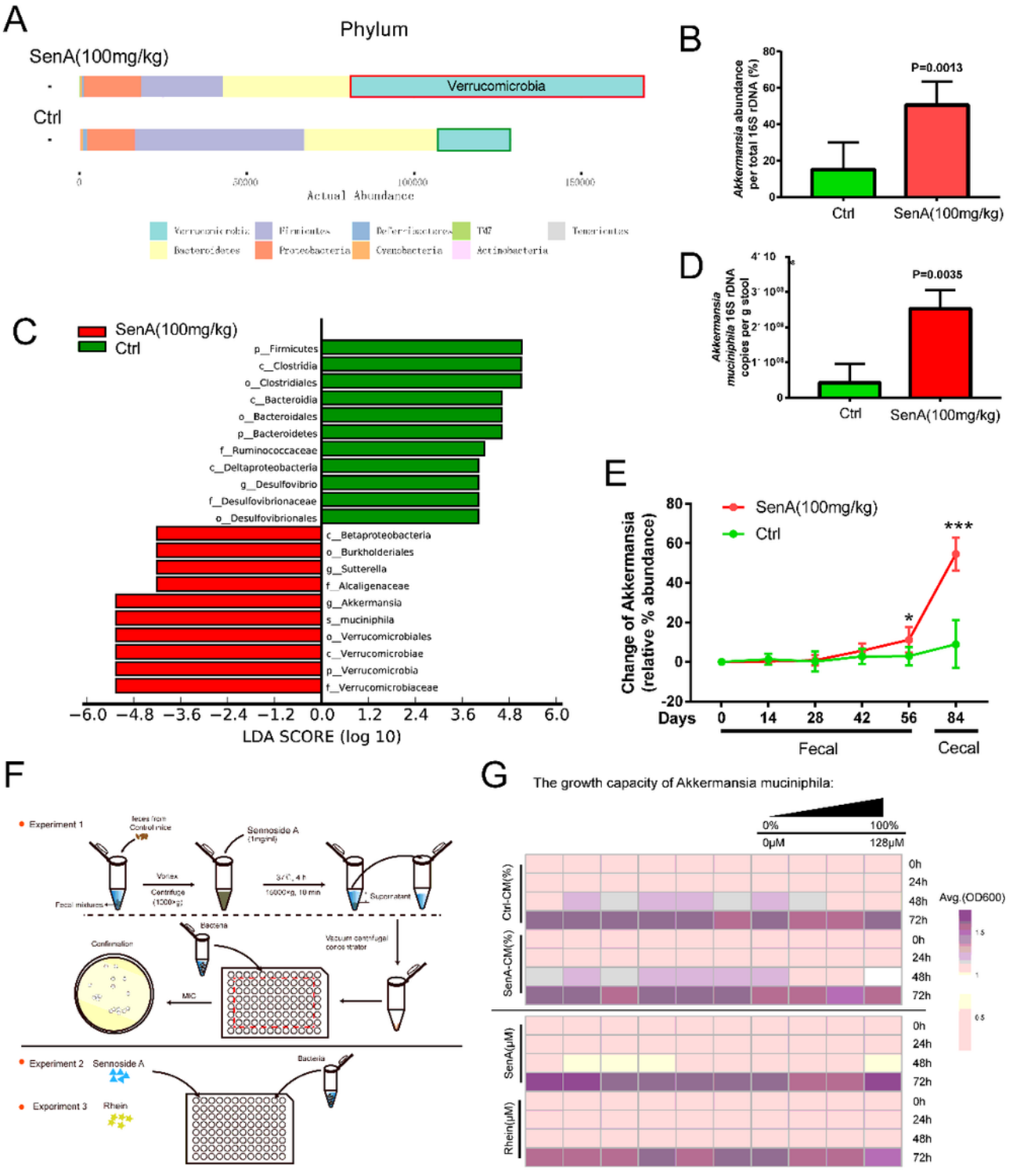

Figure 2

Sennoside A promotes enrichment of mucus-degrading bacteria. (A) Bacterial taxonomic profiling at the phylum level of intestinal bacteria from different mouse groups. (B) Relative abundance of Akkermansia. See also Figures S3. (C) 16s rDNA copies of Akkermansia Muciniphila measured by quantitative PCR. (D) Linear discriminant analysis (LDA) scores derived from LEfSe analysis, showing the biomarker taxa on at the genus level (LDA score) of >4 and a significance of P <0.05 determined by the Wilcoxon signed-rank

test. (E) Changes in relative Akkermansia abundance over time in mice oscillated for 14-day increments. Changes in Sennoside A treatment and control groups are shown for comparison. Asterisks indicate a statistically significant difference (SenA v.s. Ctrl) using student's t test. (F) Experimental design of bacterial growth assays in vitro. See materials and methods for details. (G) Heat map showing the growth capacity of Akkermansia Muciniphila strains in the respective media. The values shown are averages of OD600.

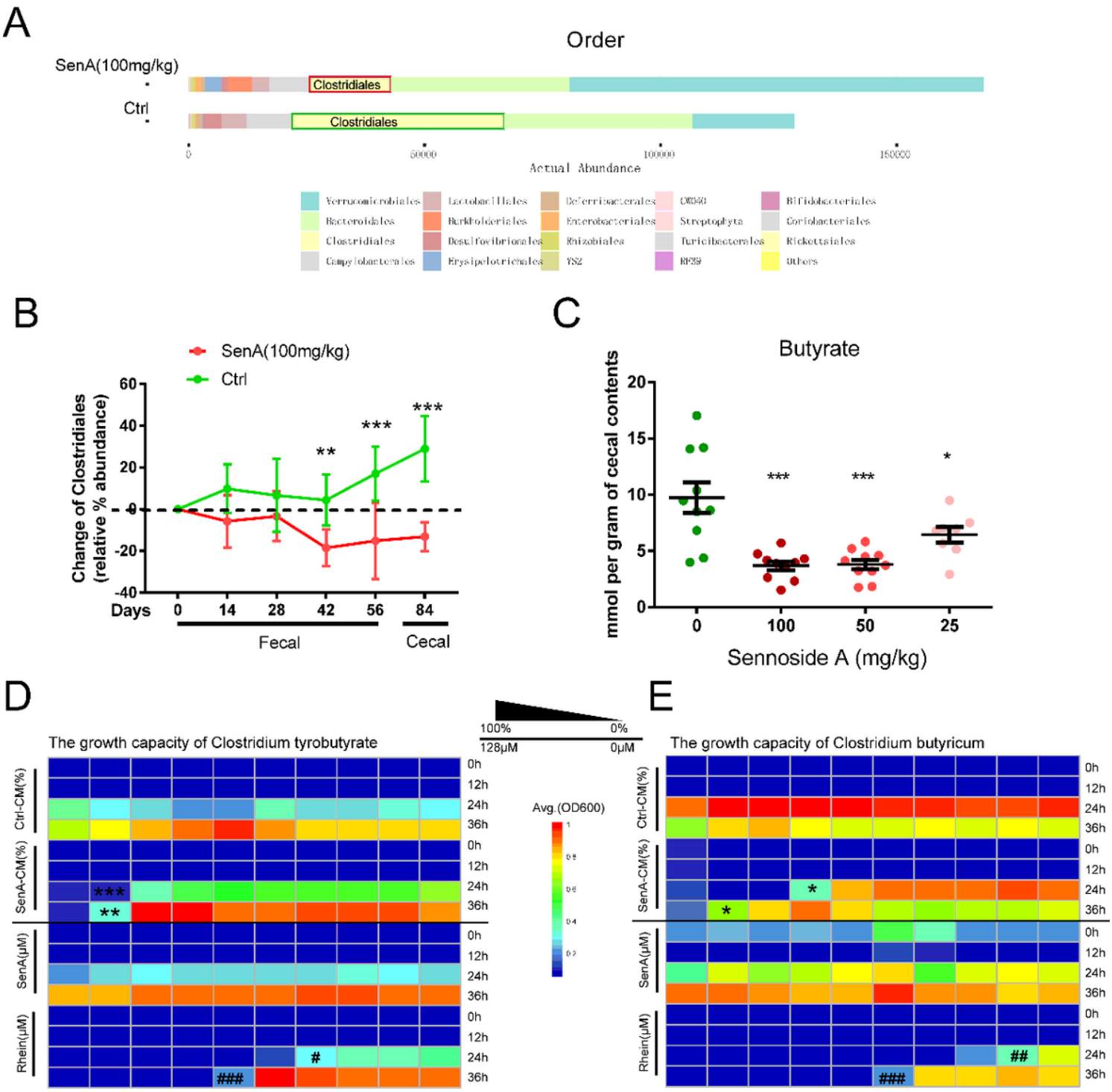

Figure 3

Sennoside A inhibited butyrate-producing bacteria growth. (A) Bacterial taxonomic profiling at the order level show that Sennside A significantly inhibited the relative abundance of clostridiales. (B) Stream plots exhibiting fecal (over time) and cecal (end point) dynamics abundance of Clostridiales.**p<0.01, ***p<0.001 versus Ctrl group at the same time points.(C) Concentrations of butyrate determined from cecal contents. Middle lines indicate average of the individual measurements shown and error bars represent SEM. One-way analysis of variance. See other short chain fatty acids also measured by GC-MS in Figure S5. (D) Direct influence of Sennoside A on butyrate-produced Clostridiales. Influence of Sennoside A and its intestinal metabolites on Clostridium tyrobutyrate (left panel) and Clostridium butyricum (right panel).

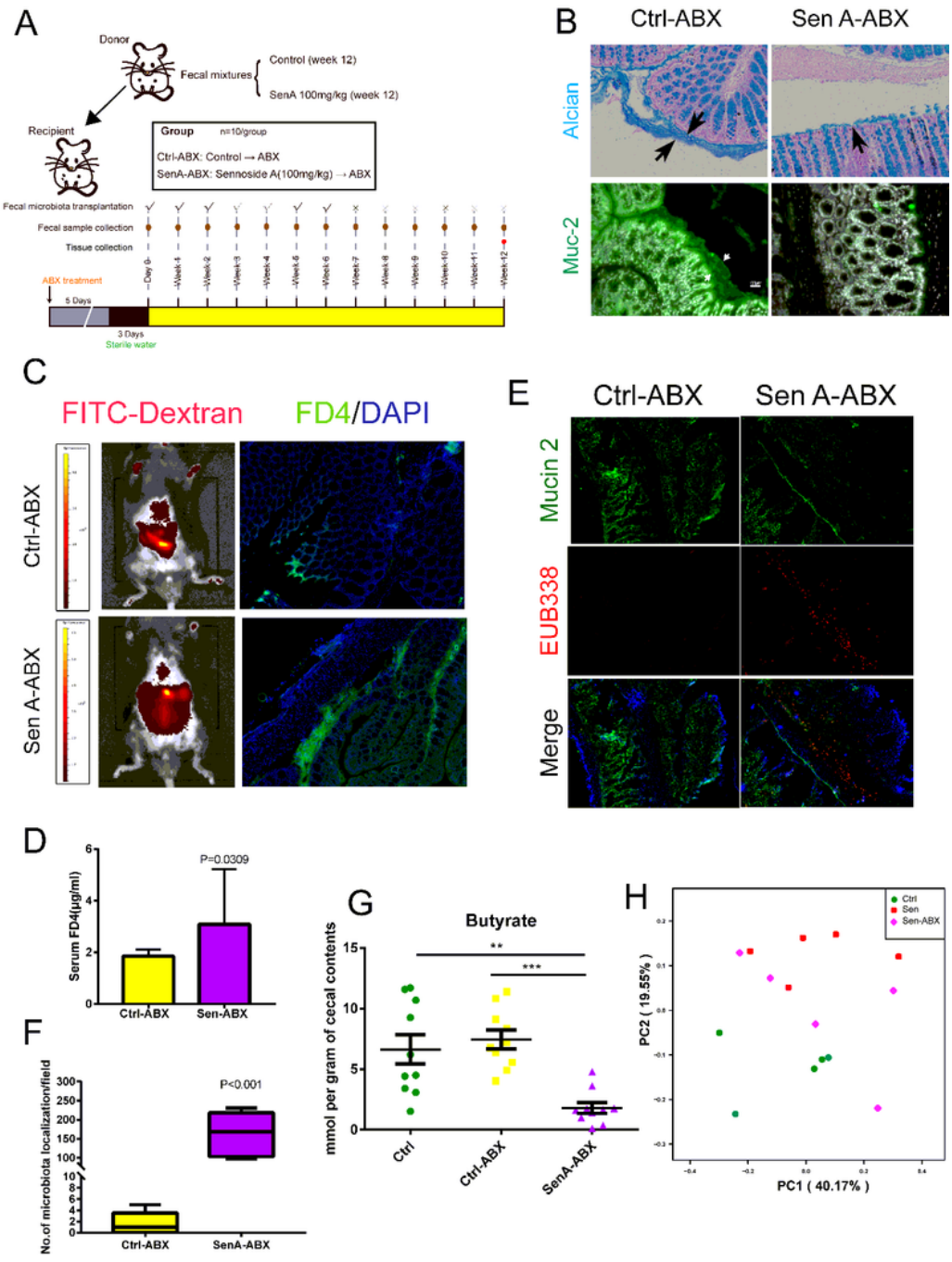

Figure 4

Sennoside A-caused gut barrier dysfunction are transferable by fecal transplantation. (A). Study design of fecal transplant experiment. See Animal protocol 2 for detailed implementation strategies. (B) Disruption of the colonic mucus layer by faecal bacteria from Sennoside A treated mouse (SenA-ABX) versus control mouse (Ctrl-ABX) detected by Muc2 immunofluorescence and Alcian blue staining. (C&D) Imaging live mice, colon sections and serum FD4 revealed that the disruption of intestinal barrier integrity were

observed in SenA-ABX mice. (E) Bacterial Translocation across the Intestinal Barrier in SenA-ABX mouse. Magnification, ×400. (F) Bacteria counts in epithelial cell intracellular. (G) Measurement of SCFAs in the colon content of SenA-ABX and ctrl-ABX mice. See also Figure S6A-E. All error bars represent SEM. ***p < 0.001; **p<0.01. *p < 0.05; ns, no significance. (H) PCoA revealed that the SenA-ABX bacterial communities clustered separately from ctrl bacterial communities, which were more similar to SenA group. Each circle represents a single sample, coloured by group.

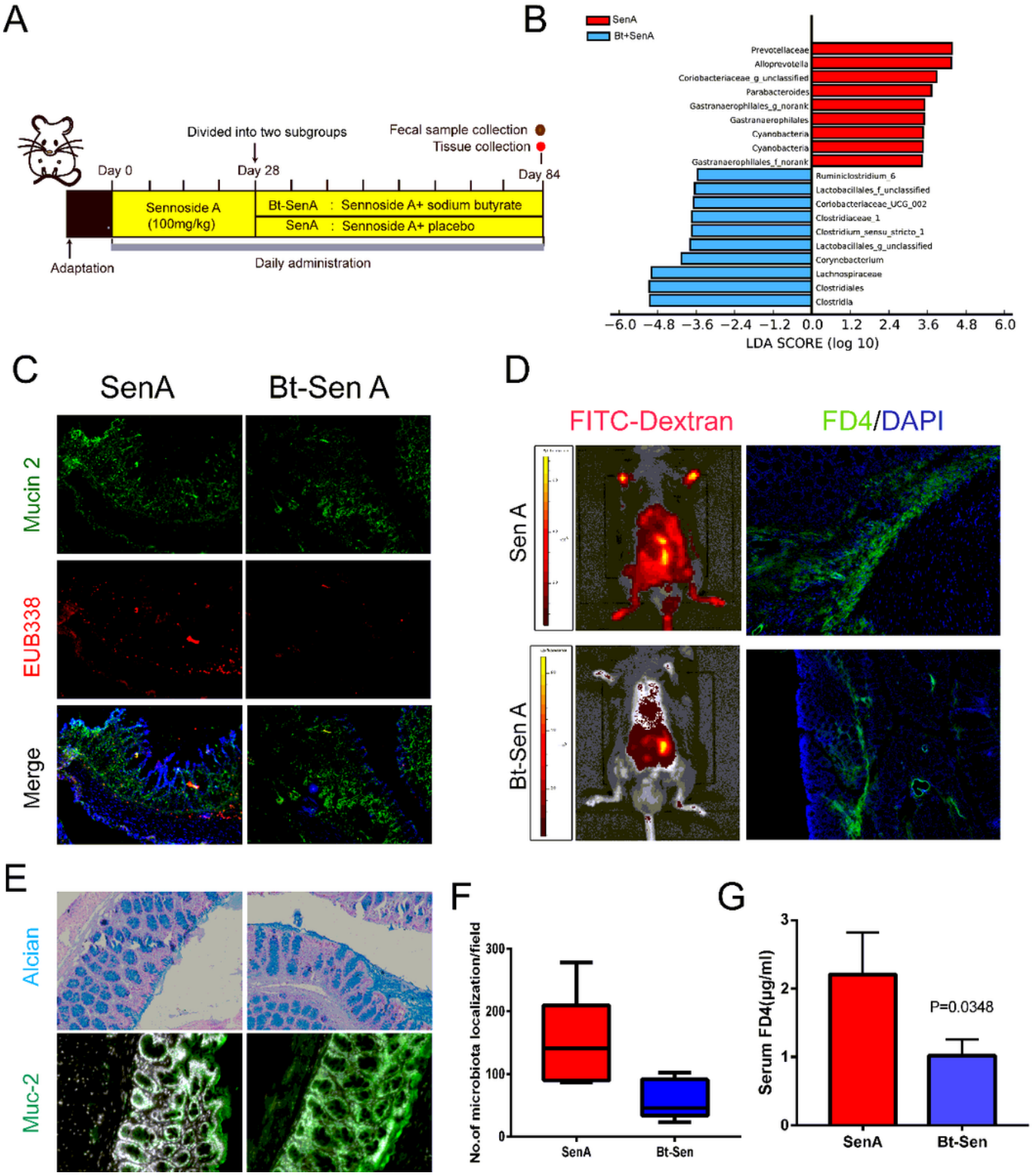

Figure 5

Oral administration of Butyrate protects mice against sennoside A-induced damage. (A)Schematic of Butyrate supplement experimental design and collection protocol. See Animal protocol 3 for detailed implementation strategies. (B) LEfSe analysis identified the most differentially abundant taxa between the two groups. SenA-enriched taxa are indicated with a positive LDA score, and taxa enriched in Bt-SenA have a negative score. Only taxa meeting an LDA significant threshold of >4 are shown. (C) Representative in situ detection of bacteria in the SenA and Bt-SenA groups. Colon tissue sections were stained with DAPI (blue), Muc2 (green) and probed with universal eubacterial probe EUB338I (red). Original magnification, ×100. (D) Evaluation of intestinal permeability. (E) Representative immunofluorescence (Muc-2) images (magnification, ×200) and Alcian blue images (magnification, ×100). (F) Comparison of total bacterial load in the field of SenA and Bt-SenA group. (G) Intestinal permeability was assessed with serum FD4.

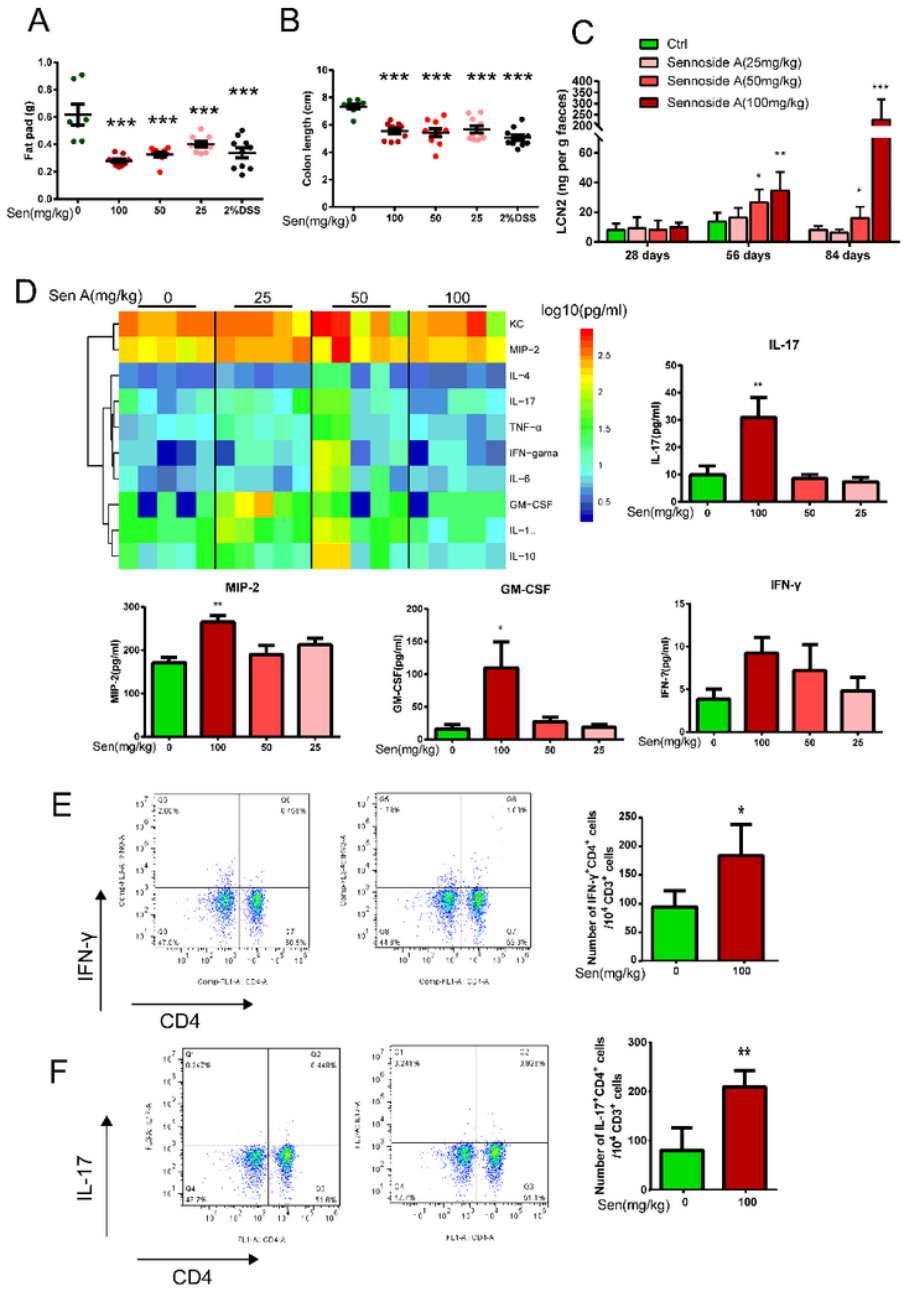

Figure 6

Long-term Sennoside A treatment induces chronic low-grade Inflammation. (A) Visceral fat pad weight (epididymal white adipose tissue) and (B) colon length were measured after 12 weeks of treatment as described in the 'Methods' section. (C) Fecal level of the inflammatory marker LCN2 in each group in differernt time-points (n=8-9 mice per group). (D) Heatmap representation of ten specific cytokine levels in serum, including CXCL1, CXCL2, IFN-γ, IL-4, IL-6, GM-CSF, IL-1β, IL-17, IL-10, and TNF-α. The color of the heatmap in each row is based on log10 (pg/mL) values(n=4-5 per group). Estimated lsmean and 95% CI are shown for selected cytokines. (D) Flow-cytometric plots of IFN-γ and IL-17 expression on fetal and infant CD4+ cells in mesenteric lymph nodes. Statistical significance was measured by one-way ANOVA or t-text. The p value is shown as *p < 0.05, **p < 0.01.

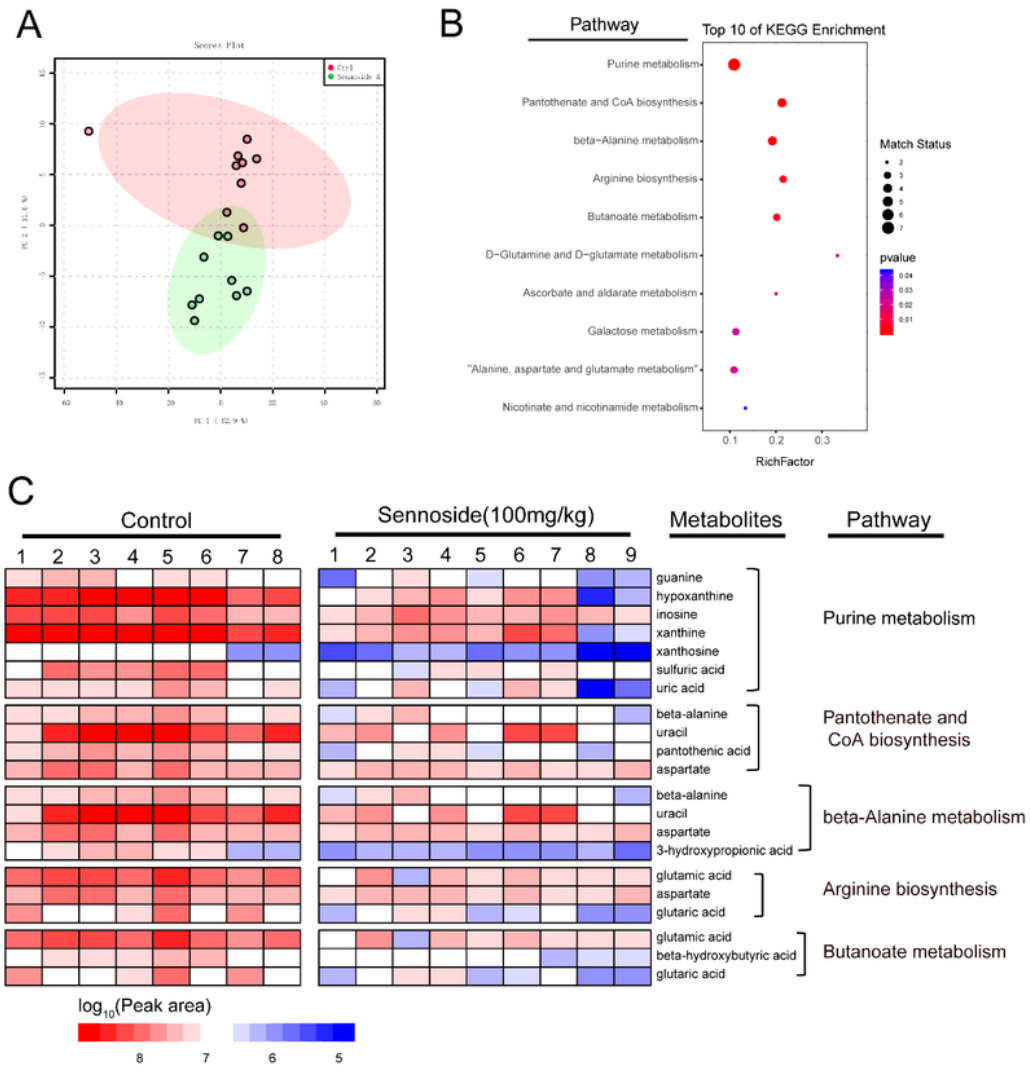

Figure 7

Key metabolites and pathway enrichment analysis based on metabolomics. (A) Principal components analysis (PCA) score plots for discriminating the fecal metabolome from ctrl and SenA (100mg/kg) groups. (B) Disturbed metabolic pathways in the Ctrl versus SenA groups. (C) Heatmaps of the differential metabolites that were contained in enriched pathways and altered by Sennoside A (100mg/kg) compared with control mice (n=8-9).The differences of abundance distributions among

metabolites between two groups were measured by GC-MS. P values less than 0.05 were considered statistically significant. See also Figure S11 and supplementary dataset S1.

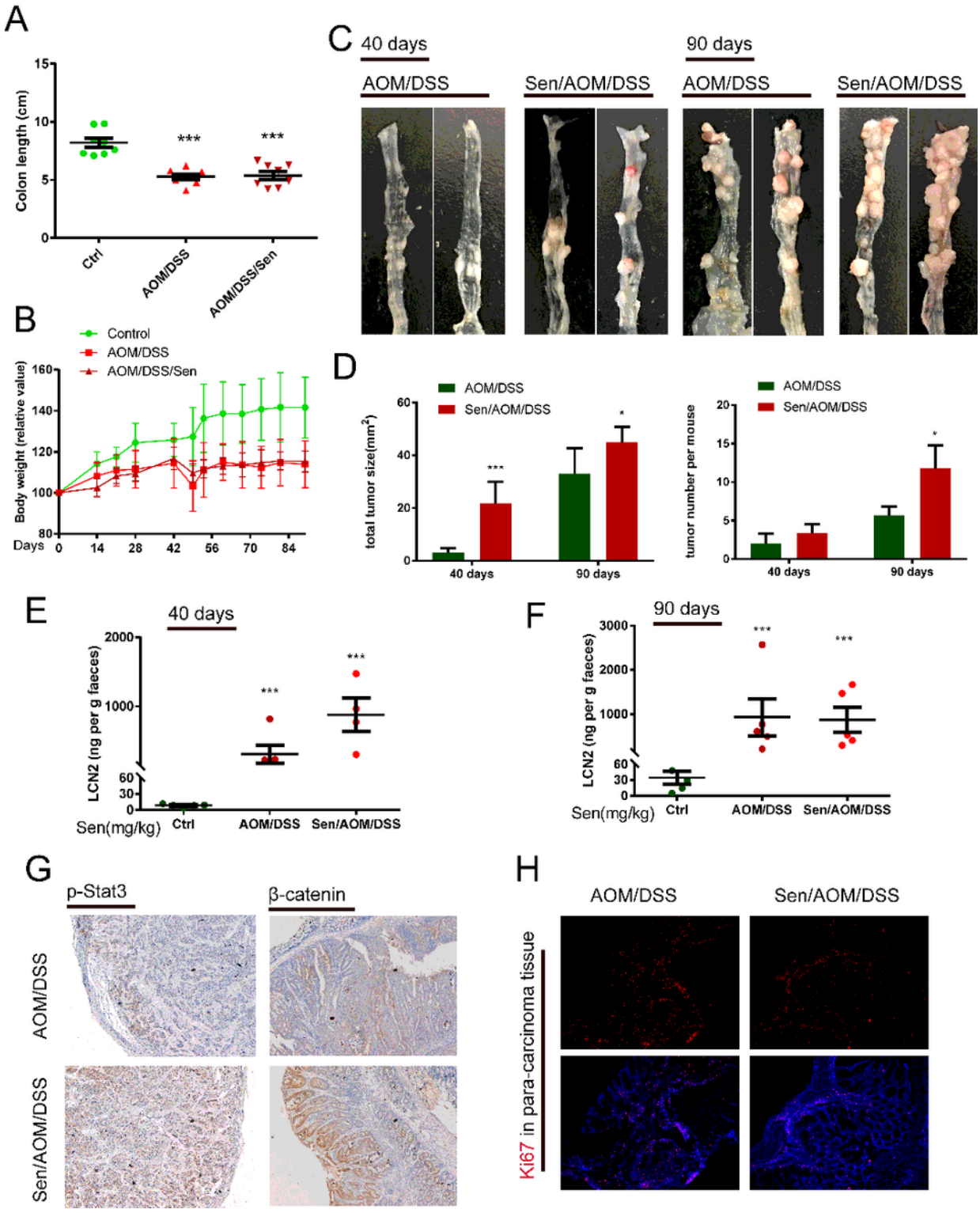

Figure 8

Inflammation-Induced Tumorigenesis is enhanced in Mice with sennoside A treatment. (A) Gross morphology and length of the large bowel in different groups. ***p<0.001 versus ctrl group. (B) Changes of body weight over a period of observation are shown as percent of the initial weight at the start of

experiments.(C) Representative image of colon in mice 40 days and 90 days after the first azoxymethane injection. (D&E) Size and Number of colon tumors. Error bars, mean hSEM. *p < 0.05,***p < 0.001 as calculated by t-test. (E&F) Faecal levels of the inflammatory marker LCN2 at day 40 and day 90 post-injection. (G) Immunohistochemical analysis of phospho-STAT3 and β-catenin expression in tumors (day 90). (H) Immunofluorescent images for detection of Ki67 in para-carcinoma tissue.

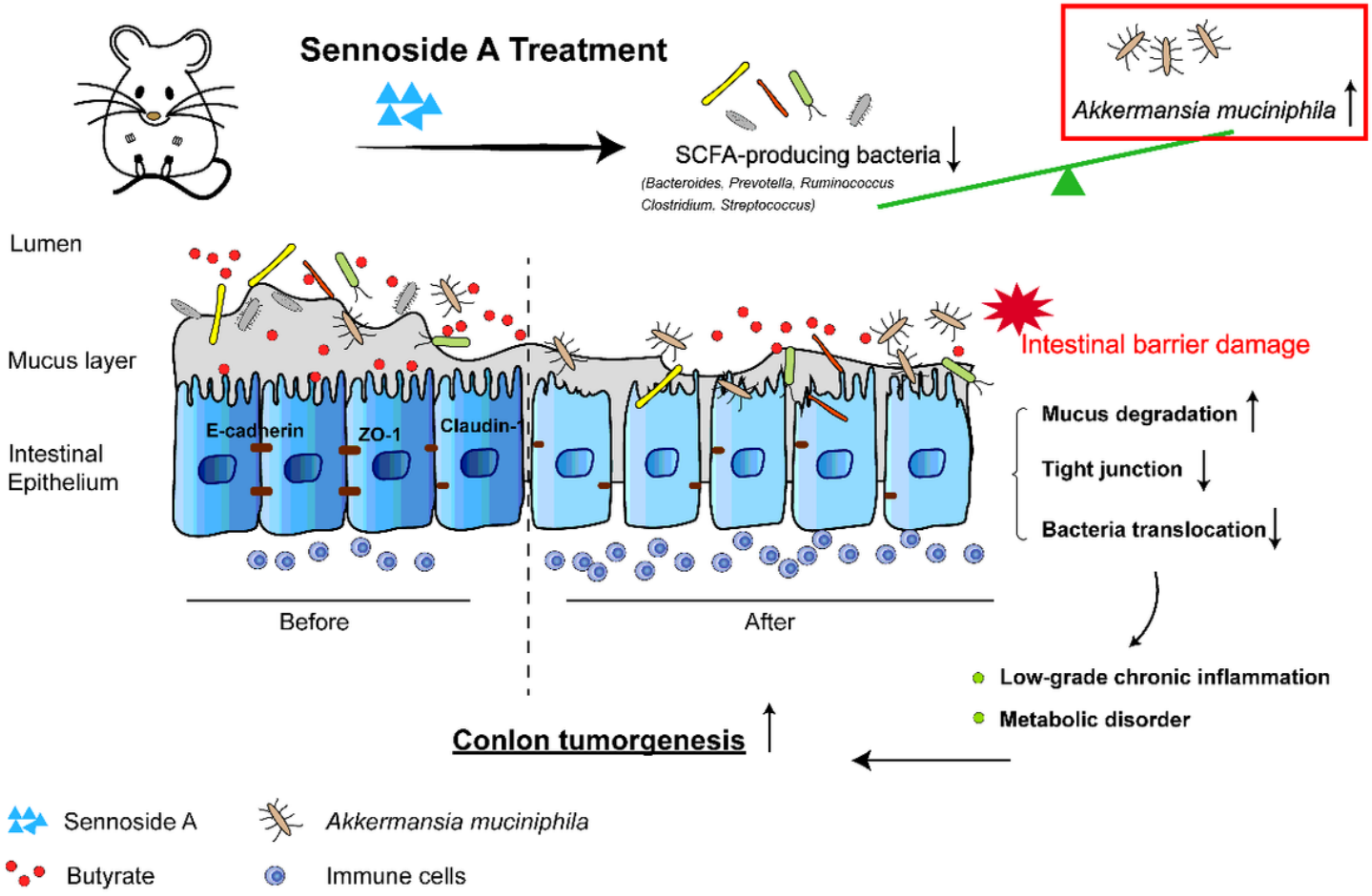

Figure 9

Graphical Abstract. Anthraquinone laxative damages colonic mucosal barrier integrity for colorectal cancer progression by upsetting the balance of intestinal microbial composition.

Supplementary Files

This is a list of supplementary files associated with this preprint. Click to download.

- SUPPLEMENTARYMATERIALS.docx
- supplementarydatasetS1.xlsx